Univerzita Karlova v Praze

3. lékařská fakulta

Doktorský studijní program v biomedicíně

Fyziologie a patofyziologie člověka

Dizertační práce

Nanotechnology in the intensive care: Intravascular biocompatibility of carbon nanomaterials – effect of carbon nanotubes on blood platelets.

Nanotechnologie v intenzivní péči: Intravaskulární biokompatibilita uhlíkových nanomateriálů – uhlíkové nanotuby a krevní destičky

MUDr. Jana Šemberová

Praha, 2012

Školitel: doc. MUDr. Zbyněk Straňák, CSc.

Prohlašuji, že jsem závěrečnou práci zpracovala samostatně a že jsem řádně uvedla a citovala všechny použité prameny a literaturu. Současně prohlašuji, že práce nebyla využita k získání jiného nebo stejného titulu.

Souhlasím s trvalým uložením elektronické verze mé práce v databázi systému meziuniverzitního projektu Theses.cz za účelem soustavné kontroly podobnosti kvalifikačních prací.

V Praze, Květen, 2012

……

MUDr.Jana Šemberová

Děkuji doc. MUDr. Zbyňku Straňákovi, CSc., Janu Šimákovi, Ph.D. a Dr. Ing. Karlu Holadovi za vedení, cenné rady a trpělivost. Dále děkuji svým kolegům z ÚPMD Podolí a Laboratory of Cellular Hematology, CBER, FDA a svým blízkým za pomoc a podoru.

Abstract

Nanotechnology in the intensive care: Intravascular biocompatibility of carbon nanomaterials – effect of carbon nanotubes on blood platelets.

EFFECT OF CARBON NANOTUBES ON BLOOD PLATELETS

Carbon nanotubes (CNTs) are among the principal materials currently used in biomedical nanotechnologies. CNTs possess superior mechanical and chemical characteristics including enormous tensile strength, elasticity and conductivity. As a result they are very popular and attractive for use in various biomedical applications. Many of these applications may lead ultimately to contact of carbon nanomaterials and blood. Furthermore, CNTs may also be present intravascularly as a result of environmental or occupational exposure. Therefore, the investigation of the intravascular biocompatibility of CNTs is a critical safety issue.

We studied the effects of structurally different purified CNT materials from different manufacturers on human platelets and compared their effects to amorphous carbon black nanoparticles (ACB), fullerene C_{60}, fullerenol $C_{60}(OH)_{24}$ and NIST standard polystyrene nanobeads (PNBs). Using light transmission aggregometry of human platelet rich plasma, we found that various CNTs induce PLT aggregation and this occurs in a concentration dependent manner. In contrast to CNTs, ball-like shaped fullerene did not cause platelet aggregation. Flow cytometry analysis showed that CNTs induce platelet activation, demonstrated by the detection of surface exposure of CD62P and CD63 and the release of $CD62P^+$ and $CD63^+$ platelet membrane microparticles (MPs). Field emission scanning electron microscopy (FESEM) and transmission electron microscopy (TEM) confirmed that the platelets in contact with CNTs undergo morphologic changes from resting discoid to activated state with pseudopodia, membrane budding and microparticle shedding. CNTs induce an increase in intracellular Ca^{2+} concentration in platelets loaded with Ca^{2+}-sensitive probe FURA-2AM, as detected by ratio fluorometry. Rapidly occurring CNT-induced extracellular Ca^{2+} influx could be inhibited by calcium channel blockers SKF 96365 and 2-APB. Investigating this phenomenon further, we observed that CNTs penetrate the platelet plasma membrane without any discernible damage but then interact with the dense tubular system (DTS) causing depletion of platelet intracellular Ca^{2+} stores as shown by electron (FESEM, TEM) and immunofluorescent microscopy. This process is

accompanied by the clustering of stromal interaction molecule 1 (STIM1) co-localized with Orai1 protein, indicating an activation of the store-operated Ca^{2+} entry (SOCE) mechanism.

To investigate the effect of size and charge of nanosized materials we used the PAMAM dendrimer model.

In conclusion, we were able to prove that CNTs induce platelet activation and aggregation and thus possess highly prothrombotic properties. Furthermore we revealed the underlying molecular mechanism of CNT-induced platelet activation. These findings are critical in the evaluation of the biocompatibility of carbon nanomaterials with blood.

Abstrakt

Nanotechnologie v intenzivní péči: Intravaskulární biokompatibilita uhlíkových nanomateriálů – uhlíkové nanotuby a krevní destičky

Uhlíkové nanotuby patří v současnosti mezi nejdůležitější nanomateriály využívané v biologii a medicíně. Vyznačují se unikátními mechanickými a fyzikálně-chemickými vlastnostmi, jako je vysoká pevnost, pružnost a výborná vodivost při minimálníich rozměrech. To z nich dělá velmi atraktivní materiály pro použití v různých oblastech biomedicíny, z nichž mnohá zahrnují přímý kontakt s krví a přítomnost nanotub v intravaskulárním prostředí. V organismu se však mohou ocitnout i z jiné příčiny – po průniku tkáněmi z kontaminovaného okolního prostředí. Výzkum intravaskulární biokompatibility těchto materiálů je tedy klíčový pro zajištění bezpečnosti jejich dalšího praktického použití.

V naší studii jsme se věnovali vlivu strukturálně odlišných uhlíkových nanotub na krevní destičky a porovnávali ho s efektem nanočástic amorfního uhlíku, fullerenu C_{60}, fullerenolu $C_{60}(OH)_{24}$ a polystyrenových nanokuliček o standardní velikosti. Agregometrií jsme prokázali , že uhlíkové nanotuby způsobují agregaci krevních destiček v lidské plasmě, přičemž míra agregace rostla s koncentrací nanotub. Polystyrenové nanokuličky a ani fulleren, jehož molekula má kulovitý tvar, agregaci krevních destiček nevyvolávaly. Analýza průtokovou cytometrií potvrdila, že kontakt s uhlíkovými nanotubami vede k aktivaci destiček, potvrzenou zvýšenou expresí aktivačních povrchových markerů CD62P a CD63 a dále uvolněním CD62P aCD63 pozitivních mikropartikulí. Elektronová mikroskopie (rastrovací a transmisní elektronová mikroskopie) potvrdila, že u krevních destiček po kontaktu s uhlíkovými nanotubami dochází k morfologickým změnám typickým pro aktivaci. Jejich tvar se mění z klidového diskovitého na aktivovaný - kulovitý s pseudopodiemi, membránovými nerovnostmi a dochází k uvolnění membránových mikropartikulí. Fluorescenční mikroskopie za použití indikátoru FURA-2AM prokázala, že kontak destiček s uhlíkovými nanotubami vede k rychlému zvýšení hladiny nitrobuněčného vápníku. Pozorované zvýšení nitrobuněčné koncentrace vápenatých iontů bylo inhibovatelné blokátory kalciových kanálů SKF 96365 a 2-APB. To naznačilo, že zvýšení hladiny nitrobuněčného vápníku není způsobeno pouhým mechanickým narušením buněčné membrány krevních destiček nanotubami. Při dalším zkoumání tohoto jevu jsme byli schopni dokumentovat průnik uhlíkových nanotub plasmatickou membránou destičky bez jejího

zjevného poškození a dále i interakci nanotub se strukturou densního tubulárního systému. Elektronová a imunoflourescenční mikroskopie prokázala, že tato interakce je zodpovědná za uvolnění nitrobuněčných zásob vápníku z densního tubulárního systému, které vede k otevření membránových vápníkových kanálů a aktivaci krevních destiček. Tento proces byl doprovázen shlukováním molekul STIM1 s molekulami proteinu Orai1 v cytoplasmatické membráně destiček, což prokázalo aktivaci mechanismu na zásobách závislého vstupu vápníku do buňky (store-operated Ca^{2+} entry (SOCE)).

Obecný efekt velikosti a náboje nanomateriálů na krevní destičky jsme dále zkoumali pomocí modelu polyamidoaminových (PAMAM) dendrimerů, materiálů, kde jsou obě tyto veličiny lehce modifikovatelné. Prokázali jsme, že dendrimery o větší velikosti s kladným nábojem, oproti dendrimerům menším a/nebo se záporným či neutrálním nábojem, způsobují agregaci destiček. Podstatou dendrimery způsobené agregace je narušení buněčné membrány krevních destiček.

V předložené práci dokazujeme, že uhlíkové nanotuby způsobují aktivaci a agregaci krevních destiček a jsou tedy značne protrombogenní. Navíc se nám podařilo objasnit molekulární mechanismus aktivace krevních destiček uhlíkovými nanotubami. Tato zjištění mají zásadní význam pro hodnocení biokompatibilty uhlíkových nanomateriálů s krví a jejich použití v biologii a medicíně.

1. Introduction and overview

1.1. Introduction

Carbon nanotubes – friend or foe?

Nanotechnology has developed very rapidly over the past number of years. It seems like "nano" is ready to enter all aspects of everyday life. The evidence is all about us: we eat food wrapped in packaging enhanced by nanomaterials to help it to stay fresh longer; we treat our skin with cosmetic products containing nanosized liposomes hoping for better results; we routinely use communication and imaging technology containing nanomaterials at work and in our home; we drive cars with plastics filled with nanotubes to increase endurance; and, we enjoy sports equipment made partly of carbon nanomaterials to improve performance.

Obviously, the field of health care is not left behind. Due to their unique characteristics, certain nanomaterials have emerged as important tools in modern medicine. Nanomaterials are gaining tremendous influence in the areas of treatment, diagnosis, monitoring and control of biological systems.

Carbon nanotubes are among the most promising nanomaterials for biomedical use. They possess qualities like superior mechanical strength, increased flexibility, large surface area, high aspect ratio and high absorbency, great thermal and electric conductivity. They have a profound impact on the development of targeted therapeutics and drug delivery carriers, diagnostic biosensors and imaging nanoprobes for intravascular use. Also, the field of tissue scaffolds, prosthetics and surgical implants, vascular stents and other devices for cardiovascular and bypass surgery, neuron growth and regeneration, various bioseparators and biofilters, biocatalysts, nanoporous membranes and dialysis systems could profit from carbon nanotubes excellent mechanical and chemical properties. Among its expected future applications are nano robots, artificial muscles and other advanced prosthetics, for example, bionic limbs.

However, new discoveries bring new hazards. Simultaneous with the growth and success of the whole nanotechnology business, the possibility of environmental and occupational exposure has increased substantially. Given the relatively low cost for the industrial production of carbon

nanotubes, production levels are continuously rising, making them readily available. Furthermore, carbon nanotubes are released into the atmosphere as a part of combustion-related pollution, which, despite various international initiatives, is not decreasing at all.

Nanoparticles pose unique environmental and societal challenges, particularly with regard to biocompatibility and toxicity.

The pulmonary toxicity of carbon nanotubes was proven in various experiments, which showed, after intratracheal instillation of the material, the development of epithelioid granulomas, together with interstitial and peribronchial inflammation. Some nanomaterials have been shown to penetrate through the skin, pass across epithelia and ultimately present in different compartments. *In vitro* experiments showed multiple adverse effects on various cell cultures, including pro inflammatory, pro apoptotic, increased oxidative stress, inhibition of cell proliferation and ultimately cell death. The question comes to mind: are we facing the "new asbestos"?

Although the interactions of nanomaterials with biological systems have been recently extensively studied, only a very few studies explore their effect in the intravascular environment. Particularly lacking are studies concerning blood platelets, cells playing vital role in hemostasis and inflammation.

Nanomaterials may be administered directly into the intravascular compartment as a part of treatment or diagnostic procedure. A nanomaterial-containing device may be implanted into the circulation or extravascular tissue. Blood could come into contact with a nanomaterial-based device or device surface extracorporally, for example, as a part of various extracorporal circulation techniques, apheresis, filtration or dialysis or simply in the tubing or device containing nanoparticles-enhanced plastics. Nanomaterials may also materialize intravascularly as a result of environmental/occupational exposure, transferred through the different points of entry, including transcutaneously, after ingestion or inhalation. Intravascularly present nanoparticles may interact with all the crucial functions of endothelia, the plasma coagulation system and blood cells, including platelets. In the worst-case scenario, this interaction may lead to development of irreversible multiple organ failure and death.

Taking into account all the available information, the area of intensive care is logically one of the first dealing with nanomaterials in medicine. We are the ones seeking to maximize all the advantages of nanomaterial-containing devices to more effectively treat our patients. Therefore, we are also the ones who will be dealing with any potential adverse affects and complications.

For that reason, we are the ones who should be among the first to study carefully the effects and interactions of this new player in our field.

1.2. Nanotechnology

Nanotechnology could be defined as the design, characterization, production, and application of structures, devices, and systems by controlled manipulation of size and shape at the nano scale. Nanotechnology deals with structures sized between 1 to 100 nanometers in at least one dimension. Nanotechnology creates products with novel/superior characteristics due to their proportion (www.nanowerk.com).

To summarize, the crucial features of nanotechnology are the size, man-made nature and having properties that only arise because of the nano dimensions (Feature. Nature Nanotechnol, 2006).

There is no single field of nanotechnology. It is more a platform, where all the other science fields, such as mathematics, biology, chemistry, physics, engineering and others meet and deal in nanoscale. Nanotechnology is not just a new field of science and engineering, but a new way of looking at and studying (Feature. Nature Nanotechnol, 2006).

Materials reduced to the nanoscale - nanomaterials - show different properties compared to what they exhibit on a macroscale. One example is the increase in surface area to volume ratio altering mechanical, thermal and catalytic properties of materials or "quantum size effect" where the electronic properties of solids are altered with great reductions in particle size. These characteristics enable unique applications but also are posing new risks (www.nanowerk.com, www.nano.gov).

1.3. Carbon nanomaterials

Carbon nanomaterials are among those with the largest number of potential or currently in use applications. The main types of carbon nanomaterials are carbon nanotubes (CNTs) and fullerenes.

1.3.1 Fullerenes

Fullerenes are allotropes of carbon of spherical shape. Originally, fullerene C60 (buckminsterfullerene) is a spherical molecule about 1nm in diameter, comprising 60 carbon atoms arranged as 20 hexagons and 12 pentagons - the configuration of a football (fig.1). There are now thirty or more forms of fullerenes, up to and beyond C120. The important fact is that useful dopant atoms can be placed inside the hollow fullerene ball (www.nanowerk.com).

1.3.2. Carbon nanotubes

Carbon nanotubes are extended family of cylindrical structure molecules related to graphene. The molecular structure of graphene is planar network of interconnected hexagonal rings of carbon atoms (which resembles to stacked, one-atom-thick sheet of chicken wire) (fig.1). When graphene sheets are rolled into a cylinder and their edges joined, they form CNTs. Two main types of nanotubes are single-walled carbon nanotubes (SWCNTs) and multiwalled carbon nanotubes (MWCNTs) according to the number of layers (fig.1). CNTs in general have large length-to-diameter ratio and come in a variety of diameters, lengths, and functional group content (surface modified - functionalized carbon nanotubes) (Kalbac et al., 2008, www.nanowerk.com, www.nano.gov).

Nanostructured carbons are not limited to nanotubes and fullerenes - they also exist as nanofibers, cones, buds, torus, scrolls, whiskers, and graphite polyhedral crystals.

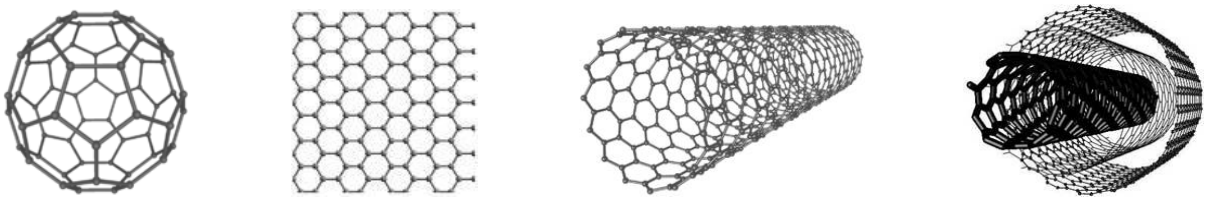

Fullerene C60 Graphene sheet Single-walled CNT Multiwalled CNT

Figure 1. Schematic representation of selected carbon nanomaterials.

(www.nanowerk.com, www.physicstoday.org)

Carbon nanotubes (CNTs) attract a lot of attention for their electronic, mechanical, optical, and chemical characteristics. They are mechanically very strong (as stiff as diamond), amazingly flexible, have large surface area, high aspect ratio and high absorbency. They can conduct electricity and heat extremely well. All of these remarkable properties give CNTs wide range of applications in materials science, electronics, chemical processing, energy management, bioengineering and many other fields. Among specific applications are conductive or reinforced plastics, field emitters, energy storage, conductive adhesives and connectors, molecular electronics, thermal materials, super strong fibers and transmission line cables, catalyst support, CNTs ceramics, air, water and gas filtration devices, various sensors (Baughman et al., 2002, www.nanowerk.com).

Some commercial products utilizing CNTs are on the today's market, they include stain resistant textiles, CNTs-reinforced tennis rackets, baseball bats, bicycle frames, and other sports equipment. CNTs based plastic packaging already exist and is used by Kraft foods, Coors Brewing company has developed new plastic-CNTs beer bottles that stay cold for longer periods of time. Samsung already sale CNT based flat panel displays. A lot of automotive plastics companies are using CNTs as well, CNTs have been added into the side mirror plastics on automobiles in the US since the late 1990s (www.nanowerk.com). Number of industrial facilities producing the CNTs is gradually increasing and the cost of some CNTs is decreasing proportionally (Baughman et al., 2002, www.nanowerk.com).

1.4. Nanomaterials in medicine

1.4.1 Applications

Due to the unique properties, in recent years, nanomaterials have emerged as important tools in the modern medicine. The current and future applications of nanotechnology in medicine are in the fields of treatment, diagnosis, monitoring, and control of biological systems. More specifically these are targeted therapeutics and carriers for drug and gene delivery targeting not only organs, but also individual cells, molecular imaging, biosensors, improved diagnostic and imaging devices, advanced tissue engineering.

1.4.2. Biomedical applications of nanomaterials other than CNTs

Quantum dots

Among the most frequently used nanomaterials are Quantum dots (QDs), nanoparticles composed of inorganic semiconductor molecules from a variety of different compounds. QDs absorb white light and then re-emit it a couple of nanoseconds later at a specific wavelength. By varying the size and composition, the emission wavelength can be tuned. The light emitted by QDs is far more intense and significantly more stable against photobleaching, thus their main area of use is optical imaging. QDs can be targeted to the organs within the body by coating the QD surface with appropriate molecules and allowing specific precise and non-invasive imaging *in vitro* and *in vivo* (Moghimi et al., 2005, Murthy et al., 2007).

Iron oxide andother superparamagnetic nanoparticles

Other nanomaterials used in imaging are superparamagnetic nanoparticles, such as iron oxide nanoparticles, which enable to visualize features that would not otherwise be detectable by conventional MRI. With their help MRI could monitor gene expression or detect pathologies such as cancer, brain inflammation, arthritis, or atherosclerotic plaques (Moghimi et al., 2005, Murthy et al., 2007).

Polymer and liposome-based systems

Among the nanoparticles applications, drug delivery is one of the most advanced. This is large part due to the success of polymer- and liposome-based drug delivery systems, many of which are in clinical use today (Murthy et al., 2007, Goldberg et al., 2007). These include polymeric micelles, dendrimers, polymeric and ceramic nanoparticles, protein cage architectures, viral-derived capsids, nanospheres, polyplexes, and liposomes.

Polymeric micelles are formed in solution as aggregates in which the component molecules are arranged in a spheroidal structure with hydrophobic cores with the mantle of hydrophilic groups. These dynamic systems, which are usually below 50 nm in diameter, are used for the systemic delivery of water-insoluble drugs.

Liposomes are closed vesicles that form on hydration of dry phospholipids above their transition temperature. They are classified according to their size and number of phospholipid bilayers – multilamellar or unilamellar.

Dendrimers are highly branched macromolecules with controlled three-dimensional architecture. Polymer growth starts from a central core molecule and growth occurs in an outward direction by a series of polymerisation reactions. Cavities in the core structure and folding of the branches create cages and channels.

Nanospheres are spherical objects, ranging from tens to hundreds of nanometers in size, consisting of synthetic or natural polymers (collagen, albumin).

Carbohydrate-ceramic nanoparticles (Aquasomes) are spherical particles. The particle core is composed of nanocrystalline calcium phosphate or ceramic diamond, and is covered by a polyhydroxyl oligomeric film.

Polyplexes/Lipopolyplexes are assemblies, which form spontaneously between nucleic acids and polycations or cationic liposomes and are used in transfection protocols (Moghimi et al., 2005).

Therapeutic and diagnostic agents can be encapsulated, covalently attached, or adsorbed on to such nanocarriers. Nanoparticulate carriers can be targeted to specific cells and locations within the body after intravenous and subcutaneous routes of injection.

Clinical use up to date

Nanoparticles have made tremendous impact in the treatment of various types of cancer, as evidenced by the numerous nanoparticle-based drugs and delivery systems (mainly polymer and liposome based), that are currently in clinical use (for example drugs Paclitaxel, Doxorubicin). Other areas where nanocarrier based therapeutics are in use are neurodegenerative diseases, where they help to overcome issue of blood brain barrier, HIV therapeutics - improving solubility, ocular disease therapies – allowing higher local drug concentations, respiratory therapy - modifying inflammatory response in respiratory diseases, and vaccines vehicles (Murthy et al., 2007).

1.4.3 Biomedical applications of carbon nanotubes (CNTs)

Carbon nanotubes certainly are among the nanomaterials with the largest amount of potential and in-use biomedical applications, thanks to the properties mentioned above – large surface area, multiple potential binding sites, excellent electrical conductivity and high aspect ratio.

Cells have been shown to grow on CNTs without excessive adhesion, potentially giving rise to applications such as tissue scaffolds, coatings for prosthetics and surgical implants, vascular stents and other devices for cardiovascular and bypass surgery, (Moghimi et al., 2005, Veetil et al., 2009) and neuron growth and regeneration (Moghimi et al., 2005, Massobrio et al., 2008).

Carbon nanotubes found enormous application in molecular electronics and bioelectronics. The electrical behaviour of CNTs promotes a large variety of biosensors for individual molecules sensing (Polizu et al., 2006), for example glucose, lactate and other small molecules, (Sun et al., 2010, Boero et al 2011) drugs and their therapeutic levels sensing devices (Carrara et al., 2011), viral particles (Jin et al., 2011), neurotransmitters, proteins, DNA and other molecules (Jin et al., 2011).

Carbon nanotubes have proven to be promising materials also in drug delivery, as part of targeted delivery systems assuring stability and possible visualization, mainly delivering anticancer therapeutics and DNA (Huang et al., 2011, Wu et al., 2008, Ruggiero et al., 2010).

Other applications are various bioseparators, biocatalysts, nanoporous carbon membranes which could find use in immunoisolation devices, pacemakers, kidney dialysis membranes, microdialysis systems, various bio-filters and other devices (Narayan et al., 2007). They found use also in optical imaging, magnetic resonance and as radiotracer contrast agents. Important are carbon nanotubes as fillers of plastic composites becoming parts of various medical devices. (Koyama et al., 2006)

Among future (according to some reports – near future) applications are nano robots, artificial muscles and other advanced prosthetics – bionic limbs.

Indeed, there are some instances where nanoparticles enable features that simply cannot be performed otherwise. However, there are multiple issues which have not been fully overcome yet like CNTs solubility, stability, aggregation, clearance kinetics in organism, protein interactions

and many others. Nanoparticles bring with them unique environmental and societal challenges, particularly in regard to biocompatibility and toxicity.

1.5. Biocompatibility of carbon nanotubes

1.5.1. Biocompatibility – definition

Biocompatibility is defined as the ability of a material to perform with an appropriate host response in a specific application (Williams 1999) or, more profoundly, as the ability of a biomaterial to perform its desired function with respect to a medical therapy, without eliciting any undesirable local or systemic effects in the recipient or beneficiary of that therapy, but generating the most appropriate beneficial cellular or tissue response in that specific situation, and optimizing the clinically relevant performance of that therapy (Williams 2008).

1.5.2. Carbon Nanotubes Biocompatibility and Toxicology

As the number of CNTs applications constantly increases, questioning and testing the biocompatibility and toxicology is becoming alarmingly important. Also, the number of industrial facilities producing the CNTs for a relatively low cost has raised and therefore, the chance of occupational and environmental exposure has increased as well (Colvin 2003).

Even though there are numbers of studies addressing toxicology issues published, it is still far less that the number of papers mentioning potential CNTs applications.

Possible adverse effects of carbon nanomaterials have been shown in numerous *in vitro* assays. Gelderman and Simak showed pro-inflammatory and pro-apoptotic effect of fullerenol C60(OH)24 on human umbilical vein endothelial cells (HUVECs) (Gelderman et al., 2008). Magrez et al. tested the toxicity of multiwalled carbon nanotubes, carbon nanofibers, and carbon nanoparticles in vitro on lung tumor cells. They observed inhibition of cell proliferation and cell death. Cytotoxicity of the materials and the effects were proven to be size-dependent and enhanced after acid treatment (Magrez et al., 2006). Manna et al. presented study of effect of single-walled carbon nanotubes on human keratinocyte cells, showing increased oxidative stress

and inhibition of cell proliferation. They suggested activation of NF-κB due to the activation of stress-related kinases by SWCNTs, also in a dose-dependent manner (Manna et al., 2005).

Unfavourable effects were shown also in *in vivo* studies targeting various systems. The pulmonary toxicity was proven in multiple experiments, for example Lam et al. demonstrated formation of epithelioid granulomas, interstitial and peribronchial inflammation after intratracheal instillation of single-walled CNTs. The effect was time and dose dependent (Lam et al., 2004). The mechanism behind these changes could be induction of oxidative stress, influence of different transcription factors with upregulation of proinflammatory protein synthesis (Lam et al., 2004, Medina et al., 2007). Some studies compare the effect of CNTs to those of asbestos, although this comparison is used more in the terms of underestimated thread (Shvedova et al., 2009). Also skin and other epithelia proved to be surprisingly permeable to nanomaterials with diverse physicochemical properties as shown by Rouse et al. and Ryman-Rasmussen et al. on example of nanoparticles of different origin (Shvedova et al., 2009, Rouse et al, 2007, Ryman-Rasmussen et al., 2006).

1.5.3. Carbon Nanotubes Biocompatibility Testing

As all other devices or pharmaceuticals, nanoparticles intended for biomedical application must be subject to biocompatibility testing.

The unique physicochemical properties of nanoparticles may cause unexpected interactions and interference with conventional toxicology assays (Dobrovolskaia et al., 2008 and 2010, Oberdorster et al., 2005). Physicochemical properties that may be important in understanding the toxic effects of test materials include particle size and size distribution, agglomeration state, shape, crystal structure, chemical composition, surface area, surface chemistry, surface charge, and porosity. Nanoparticles interaction with plasma proteins and blood components has to be taken in account. Qualitative and quantitative changes in nanoparticles biokinetics in a diseased or compromised organism need also to be considered.

The key elements of the toxicity assessment are: Physicochemical Characteristics, *In Vitro* Assays (cellular and non-cellular), and *In Vivo* Assays (Oberdorster et al., 2005), ideally including "second hit" model. Although numerous efforts to define the critical parameters for nanoparticle biocompatibility are currently under development, very few standardized protocols

are currently available. (Dobrovolskaia et al., 2008, Oberdorster et al., 2005, Hall et al, 2007, Fitzgerald et al., 2011). These protocols are scarce particularly in the field of cardiovascular biocompatibility despite increasing number of potential intravascular application of nanomaterials.

1.5.4. Standard intravascular biocompatibility assays

According to the ISO normative 10993-4:2002 Biological evaluation of medical devices - Part 4: Selection of tests for interactions with blood (ISO 10993-4:2002), the recommended assays testing intravascular compatibility target thrombosis, coagulation, platelets and platelet function, hematology parameters including hemolysis, and complement activation. The ISO states that the exposure of blood to device materials should be carried out under standardized conditions. However, there are currently no recommended guidelines for nanomaterial testing taking in account their specific properties and possible traditional test modifications. Thus, studies published on the topic so far are hard to compare and draw the conclusions from. Dobrovolskaia et al. recently published standard test method for analysis of nanoparticle haemolytic properties in vitro (Dobrovolskaia et al., 2008) and her group is working on multiple other protocols for nanoparticle testing (Neun et al., 2011, Dobrovolskaia et al., 2010).

1.5.5. Intravascular biocompatibility of carbon nanotubes

Any foreign material present in the intravascular compartment, unless optimally biocompatible, induces a complex response. The material recognized as a pathogenic factor (insult) elicits the defense process at the tissue level known as the acute inflammatory response. Main components in the inflammatory process induced by intravascularly exposed nanomaterials would be endothelial cells of the vessel wall, platelets, white blood cells (particularly neutrophils, monocytes, tissue residential macrophages and mast cells), red blood cells, plasma coagulation system, and complement system.

At a certain level of intensity, systemic inflammatory response progresses to multiple organ dysfunction (MODS). MODS is associated with a failure of adequate perfusion of vital organs due to microcirculation disorders including oedema, microthromboses, and other thrombohaemorrhagic complications, possibly leading to the irreversible impairment (Simak, 2009).

The interaction of a foreign material *in vivo* with blood and vessel wall is always complex, although the effect on particular components may be more apparently manifested (Simak, 2009). Focusing on interaction with platelets, the exposure to nanomaterial may possibly lead to the disorder in platelet count and functions and corresponding clinical manifestations. In the worst case scenario, platelet interaction with nanomaterial may result into development of multiple organ dysfunction and death (fig.2).

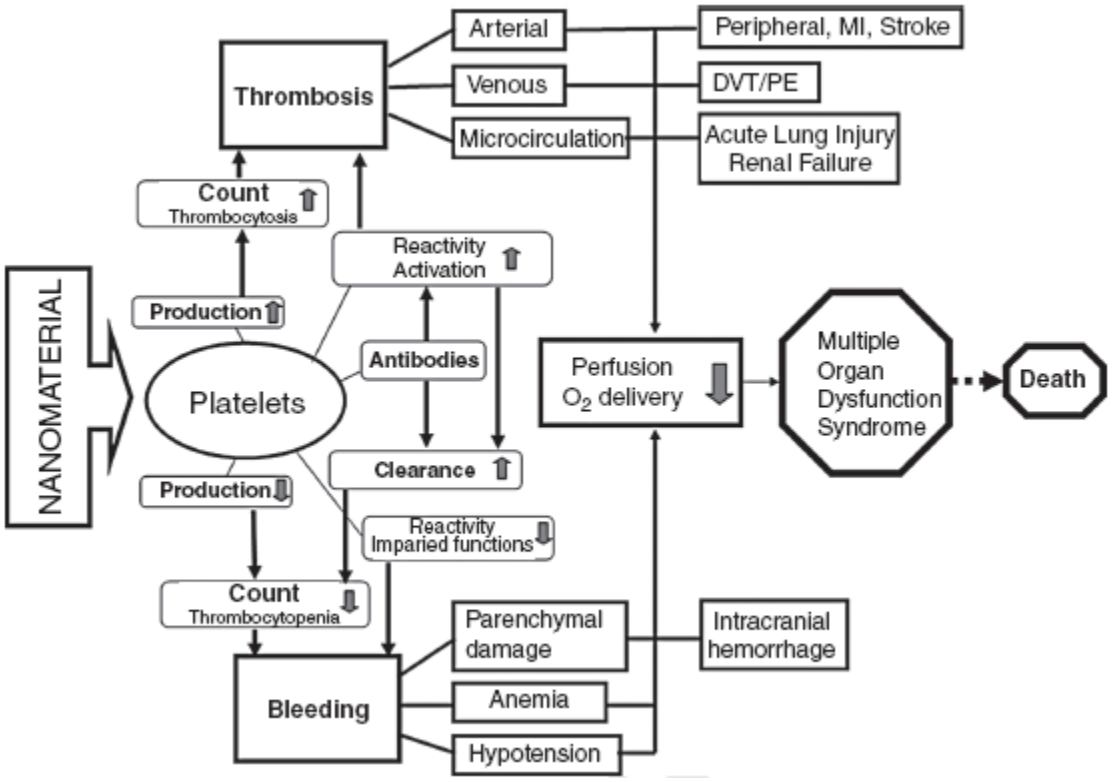

Fig.2. Possible in vivo serious adverse effects of nanomaterial interactions with platelets. MI, myocardial infarction; DVT, deep venous thrombosis; PE, pulmonary embolism. (Simak, 2009). Published with courtesy of the author.

Carbon nanotubes may come into the contact with blood components and vessel wall after the direct intravascular administration of drug delivery or diagnostic component, or indirectly as carbon nanotube containing filters, prosthetics or other medical devices exposed to blood. They may also enter the organism by inhalation, ingestion or transdermally as a result of

environmental exposure and then quickly translocate into the other compartment (Nemmar et al., 2002) and ultimately present intravascularly.

Therefore, intravascular biocompatibility of carbon nanotubes is a critical issue.

1.6. Blood platelets

Platelets are small anucleated discoid cells, of size approximately 2–5μm × 0.5μm and volume of 6 –10fl. They are produced by megakaryocytes in the bone marrow by the extension of dynamic protrusions into microvessels, sheared into the microcirculation resulting in the appearance of proplatelets in peripheral blood (Junt et al., 2007). Platelets circulate for about 10 days in the blood stream before they are cleared by macrophages in spleen and liver. Normal platelet count in peripherial blood is 150-450x10^9/L, there is a storage pool in spleen from where platelets can be rapidly mobilized.

Platelets are the key elements of hemostasis. They are very reactive with large amount of surface receptors for various activation and inhibition agonists. After the activation via different pathways, ultimately leading to the increase in intracellular calcium, platelet shape changes from discoid to spherical, pseudopodia are formed and further spreading, adhesion and aggregation occurs. Activated platelets expose phosphatidylserine on the plasma membrane, providing procoagulant surface for activation of plasma coagulation system.

In addition, activated platelets release various soluble mediators from different types of granules and membrane microparticles. Membrane microparticles (MPs) are phospholipid vesicles of about 0.1-1 μm in size released from plasma membrane of stimulated platelets and other cell types (Simak et al., 2006). Platelet MPs also expose various platelet membrane antigens and a majority of platelet MPs also exposes phosphatidylserine.

All these events are crucial to prevent posttraumatic blood loss by providing a platelet plug that leads to the closure of smaller defects of the vessel wall and are required for primary hemostasis. On the other hand, uncontrolled thrombus formation can lead to vascular occlusion and ischemia of vital tissues and organs (Simak, 2009, Varga-Szabo et al., 2008).

Platelets play important roles in other processes beyond hemostasis and thrombosis. They are strongly involved in various stages of inflammatory response and participate in the host defense of pathogens, regulation of vascular tone and integrity, wounds healing and tissue regeneration. Platelets also contribute to tumor growth and metastasis (Simak, 2009, Smyth et al., 2009).

Engineered nanomaterials can potentially interfere with different steps of platelet activation, aggregation and overall haemostasis and also influence all the other platelet functions, as schematized in fig.2. There are several methods evaluating platelet functions - activation, adhesion, aggregation and release reaction – based on different principles. Most of them can be, with possible modifications, used for nanomaterial-platelet interactions testing. However, one has to bear in mind that nanomaterials may interfere substantially with some methods. Up to date, there is no standard panel of platelet assays for nanonamerials available. The methods used in present study are described in "materials and methods" section.

1.7. Carbon nanotubes and blood platelets – literature review

As previously mentioned, there is a lack of publications questioning interactions between platelets and carbon nanomaterials and their biocompatibility. The key study on effects of carbon nanomaterials on platelets was published in 2005 by Radomski *et al.* (Radomski et al., 2005). They investigated the effects of multiwalled (MWCNT) and single-walled (SWCNT) carbon nanotubes, C60 fullerenes (C60) and mixed carbon nanoparticles (MCN, a mixture of amorphous carbon with approximately 7% C60) in the doses of 0.2–300 μg/ml on human blood platelets *in vitro* and thrombus formation *in vivo*. The materials were suspended in Tyrode's solution, sonicated and vortexed prior testing. Unfortunately, the authors did not show the size distribution of the tested materials. Nanoparticles (NP) were compared with standard urban particulate matter (SRM1648, average size 1.4 μm). The investigators performed aggregation studies using washed platelets resuspended in Tyrode's solution, preincubated with various inhibitors (prostacyclin, S-nitroso-glutathione, aspirin, 2-methylthio-AMP, phenanthroline, EDTA and Gō6976). Platelet aggregation was assayed in a whole blood ionized calcium lumi-aggregometer, monitoring also ADP release measured by luciferin-luciferase assay. Radomski *et al.* performed phase contrast and immunofluorescent microscopy and transmission electron microscopy (TEM). For these

assays, platelet aggregation was terminated at 20% of maximal response, as determined in the aggregometer, and the samples were fixed and evaluated by one of the method. The investigators also performed flow cytometry of the platelet surface expression of activated GPIIb-IIIa (PAC-1), GPIb and CD62P, or beta3 integrin (GPIIIa, CD61) using nonfixed diluted samples. Zymography of gelatinase activities in the platelet releasate was performed using SDS-PAGE with copolymerized gelatin. Activities of platelet gelatinases MMP2 and MMP9 were identified by their molecular weight and quantified by reference standards.

The study reported that mixed carbon nanomaterials (MCN), carbon nanotubes (SWCNT and MWCNT) and SRM1648 caused activation and aggregation of human platelets (MCN≥SWCNT>MWCNT>SRM1648). Interestingly, nC60 fullerene did not activate platelets. Compared to a strong platelet response to MCN, carbon nanotubes caused partial aggregation with little or no granular release. SRM1648, MCN, MWCNT and SWCNT induced activation of GPIIb-IIIa and treatment with EDTA completely inhibited aggregation, indicating the essential role of this integrin complex. MCN caused maximum aggregation response and platelet degranulation associated with ADP release. In agreement with this result, MCN-induced aggregation was inhibited by P2Y12 receptor antagonist 1-MeSAMP. In addition, MCN, but not other carbon nanomaterials, induced increased surface expression of CD62P and decreased GPIb, markers of platelet activation. All carbon NP-induced aggregation was inhibited by prostacyclin, and with less efficacy also by S-nitroso-glutathione (endogenous NO donor), but not by aspirin. A classical protein kinase C inhibitor Gō6976 did not affect MCN, SWCNT and MWCNT-induced aggregation.

Phenanthroline, which inhibits the MMP gelatinase dependent pathway of aggregation, significantly reduced the aggregation response to carbon nanoparticles. Moreover, all carbon NP tested, including nonaggregating nC60, released cytosolic gelatinases - proaggregatory MMP-2 and antiaggregatory MMP-9 from platelets. The authors suggest that the release of MMP-9 may be a sensitive index of cell exposure to nanoparticles. Although maximum aggregation response was observed *in vitro* at concentrations >100 μg/ml, the detection of activated GPIIb-IIIa or MMP-9 zymography was positive at concentrations 4–100 fold lower.

The prothrombotic effect of nanoparticles was confirmed in rat thrombosis model *in vivo*. Vascular thrombus amplification and acceleration of thrombus formation was observed after

stimulation with MCN, SWCNT, and MWCNT. SRM was less effective and no change in thrombogenesis was observed in case of C60.

Authors discussed different characteristics of carbon NP, which may impact their ability to activate and aggregate platelets like the size of particles, shape and surface characteristics. Tested carbon nanomaterials form a polydisperse suspension in aquatic solvents, forming agglomerates up to tens of μm in size. In this study, authors did not find a clear relationship between size of agglomerates and platelet-aggregating potency. Regarding shape, nanotubes may form interplatelet bridges, and thus promote aggregation, while spherical fullerenes may not. This is true for single molecules, however, may not be such when considering the agglomerates formation. Also surface characteristics, including surface charge, are different among carbon nanomaterials and may play an important role in interaction with certain surface receptors of platelet and other cell types. The effect physico-chemical characteristics, particularly the size and surface area were found important in the study of Monteiller *et al*. (Monteiller et al., 2007). Authors confirmed that nanoparticles of the larger surface area were able to elicit inflammatory response of higher intensity comparing to the particles of the identical chemical composition, same mass but smaller surface, suggesting the key role of surface area in ultrafine particle inflamogenicity.

Another important factor is the level of contaminants, particularly transition metals, which can cause an increase in ROS generation. Soluble contaminants were unlikely to affect NP aggregatory potency in Radomski *et al.* study, since the aggregating ability of particles was greatly reduced following filtration through a 100 nm filter. However, the level of purity and careful material characterization should always be part of any nanomaterial study since the effect of contaminants may be crucial.

Bihari *et al*. published another study on nanoparticle-platelet interaction, comparing the effect of diesel exhaust particulate (DEP) matter, titanium dioxide rutile, and single-walled carbon nanotube (SWCNT) to amine- and carboxyl-modified polystyrene nanoparticles of 60 nm diameter on platelet activation in vitro and on macro- and microcirculatory thrombus formation in vivo (Bihari et al., 2010). Platelet activation was evaluated using flow cytometry CD62P (P-selectin) expression measurement after incubation of whole human blood with DEP (0.1 mg/mL), titanium dioxide (0.1 mg/mL), SWCNT (0.001-0.1 mg/mL) and polystyrene

nanoparticles (0.1 mg/mL). ADP was used as positive control. Carboxyl modified polystyrene, DEP, and TiO2 nanoparticles did not change CD62P expression on platelets as compared to controls (vehicle). In contrast, ADP, amine-modified polystyrene and SWCNT nanoparticles increased significantly CD62P expression on platelets.

The role of P-selectin was emphasized also by Nemmar *et al*. (Nemmar et al., 2007), describing P-selectin mediated enhancement of peripherial thrombogenicity after CNTs inhalation exposure in mice.

As an additional marker of platelet activation, the formation of platelet–granulocyte complexes was analyzed by Bihari *et al*. Similar to the results from the CD62P expression measurements, ADP, amine- modified polystyrene, and SWCNT nanoparticles significantly increased the percentage of CD41 positive events in the granulocyte gate (CD15-positive gate). In contrast, carboxyl-modified polystyrene, DEP, and TiO2 nanoparticles had no effect on the number of platelet–granulocyte complexes. SWCNT, but no other studied nanomaterials, were also able to induce platelet aggregation assessed by light transmission aggregometry. For in vitro experiments with the whole blood, nanoparticles in this study were dispersed in the solution containing 1.5 mg/mL of human serum albumin. We could speculate that nanoparticles may interact with albumin first (Lacerda et al, 2010) and the further reactivity may be somehow influenced by this interaction.

Bihari et al. also performed in vivo experiments. Upon systemic administration of nanoparticles (1 mg/kg) to anesthetized mice, ferric chloride-induced thrombus formation was measured in small mesenteric arteries using *in vivo* microscopy. In separate experiments, DEP (1 mg/kg), titanium dioxide (1 mg/kg), or single-walled nanotubes (0.01–1 mg/kg) were injected into anesthetized mice and light/dye-induced thrombus formation was investigated in the cremasteric arterioles. Single-walled nanotubes significantly reduced the occlusion time in mesenteric arteries as well as in cremasteric arterioles representing macro- and microcirculation respectively.

In conclusion, the study of Bihari *et al*. confirms the fact that single-walled carbon nanotubes, but not diesel or titanium dioxide nanoparticles, induce platelet activation *in vitro* and exert prothrombotic effects in the circulation.

Studies on soluble C60 derivatives could further elucidate the effects of fullerenes on platelets, eliminating problems with formation of different types of agglomerates. When a fullerene molecule is hydroxylated it becomes soluble in aquatic solvents. Niwa and Iwai (Niwa and Iwai, 2007) studied the effects of a polyhydroxylated soluble derivative of C60 – fullerenol C60(OH)24 – compared with amorphous carbon black (ACB) on rabbit platelets. They used a method of whole blood screen filtration pressure aggregometry. The effects of ACB or C60(OH)24 on ADP-induced platelet aggregation in whole blood was evaluated. ACB and C60(OH)24 alone did not induce platelet aggregation. However, when whole blood was pretreated with C60(OH)24, ADP-induced aggregation threshold index values were elevated in a dose-dependent manner. In contrast, collagen- and thrombin-induced platelet aggregation was not affected. Although these results indicate that C60(OH)24 specifically facilitates ADP-induced platelet aggregation, we were not able to confirm this conclusion with our experiments using light transmission aggregometry of human PRP. In our hands, pretreatment of human PRP with C60(OH)24 had a significant inhibitory effect on ADP-induced PLT aggregation (unpublished results). These controversial results emphasize the role of experimental settings.

The studies published so far showed that carbon nanomaterials, particularly carbon nanotubes (CNTs) cause platelet activation and have prothrombogenic effect. However, studies exploring particular effects of CNTs in contact with intravascular environment and components of circulating blood remain scarce, especially in the field of platelets. In addition, molecular mechanisms of CNT effects on platelets have not been elucidated, which we found extremely challenging.

2. Project goals

The overall goal of the project is to contribute to the elucidation of the mechanism of prothrombotic effect of carbon nanotubes by investigating their interaction with blood platelets.

The specific goals are as follows:

2.1. Evaluation of the effect of different types of carbon nanomaterials on blood platelets using light transmission aggregometry.

2.2. Flow cytometry assessment of platelet activation and microparticles release induced by carbon nanotubes.

2.3. Electron microscopy characterization of carbon nanotubes interaction with platelets.

2.4. The role of calcium influx in CNT-induced platelet activation: evaluation of changes in intracellular calcium after platelet contact with carbon nanotubes using ratio fluorometry.

2.5. Investigation of the underlying molecular mechanism of CNT-induced platelet activation: Assessment of possible involvement of store operated calcium entry by direct visualization of its major components, STIM1 and ORAI1 proteins.

2.6. Evaluation of the effect of nanoparticle charge and size on platelets-nanoparticles interactions: PAMAM dendrimers model.

3. Materials and methods

3.1. Carbon nanotubes

We have studied the effects of structurally diverse purified CNTs on human platelets (PLTs) and compared their effects to amorphous carbon nanopowder (ACN), C60 fullerene (nC60), fullerenol (C60(OH)24), and standard polystyrene nanobeads (PBs). Carbon nanomaterials were purchased from various manufacturers and their purity ranged from 90-99%. All the tested materials are listed in Table1.

Nanomaterial	**Abbrev.**	**Manufacturer**	**Minimal Purity**	**Outer Diameter**	**Length**	**Aggreg. activity***
Amorphous carbon nanopowder	ACN	Sigma-Aldrich	>99%	~ 30nm	N/A	+
SWCNT	S15	SES	>90%	<2nm	5-15μm	+++
MWCNT	M60	SES	>95%	60-100nm	1-2μm	+++
Fullerene C60	nC60	MER	99.9%	~0.7nm	N/A	-
Fullerenol C60	C60(OH)24	MER	N/A	~1.3nm	N/A	-
MWCNT	M15	NanoLab	>95%	15 +/- 5nm	1-5μm	+
MWCNT-hollow structure	MH	NanoLab	>95%	30 +/- 15nm	1-5μm	+++
MWCNT-bamboo structure	MB	NanoLab	>95%	30 +/- 10nm	1-5μm	+
MWCNT-functionalized COOH	MF(COOH)	NanoLab	>95%	15 +/- 5nm	1-5μm	++
MWCNT-functionalized NH2	MF(NH2)	NanoLab	>95%	15 +/- 5nm	1-5μm	+++
SWCNT	S30	NanoAmor	>95%	1-2nm	5-30μm	+++
NIST standard polystyrene nanobeads	PB20 PB200	Duke Scientific	N/A	20nm 200nm	N/A N/A	- -

Table 1. List of tested materials. *Semiquantitative evaluation of platelet aggregating activity. Maximum platelet aggregation 0-5%, - ; 6-15%, + ; 16-25%, ++ ; >25%, +++. All materials were tested at concentration 100 μg/mL. MWCNT, multiwalled carbon nanotubes; SWCNT, single-walled carbon nanotubes; SES, SES Research, Houston, TX, USA; MER, Materials and Electrochemical Research Corporation, Tucson, AZ, USA; NanoLab, Nanolab Inc., Waltham, MA, USA; NanoAmor, Nanostructured and Amorphous Materials, Inc., Houston, TX, USA; Duke Scientific, Duke Scientific Corp., Fremont, CA, USA; N/A, not available

We confirmed the purity and the structure of all tested materials by transmission electron microscopy (TEM) analysis, since, as the literature indicates, it has been difficult to purify CNTs and to quantitate their purity, especially the amorphous carbon content and residual metal catalysts (Brukh et al., 2008, Hou et al., 2006). Carbon nanomaterials were analyzed by TEM at 20,000 times magnification. The images were measured on a Philips EM 400T* microscope operating at 120 kV equipped with a Soft Imaging System CD camera (Cantega 2K). Nanomaterial suspensions were prepared as described below. For better dispersion for TEM analysis, 2% of polyethylene glycol was used. TEM samples were prepared by dropping diluted solutions onto ultrathin carbon-coated copper grids (~3 nm) *(pictures available in supplement B)*. In order to study interactions of pristine CNTs, amorphous carbon, and C60 fullerene with platelets, these materials were tested as polydisperse suspensions prepared by minimal sonication to allow platelet contacts with material surface but to avoid its chemical changes. In our experiments, materials were resuspended to a concentration of 1 mg/mL in phosphate buffered saline and sonicated immediately prior to use for 1 min at 30 W output, frequency 20 kHz (Tekmar Sonic Disruptor, Cincinnati, OH). In platelet activation experiments, the sonicated suspensions were immediately added to the platelet rich plasma (PRP) to final concentration of nanomaterial 100 µg/ mL. Macroscopic aggregates of CNTs readily formed after sonication.

To characterize the size distribution and shape of the nanomaterial agglomerates under our experimental conditions, we performed flow particle image analysis of nanomaterial suspensions in plasma using FPIA 3000 (Sysmex, Kobe, Japan, provided by Malvern Instruments, Columbia, MD). The analysis showed that nanomaterials formed polydisperse agglomerates of a median size 0.7-2.7 μm, depending on the type of nanomaterial. We also confirmed that the tested materials (M60, ACN, nC60) did not progressively agglomerate in plasma during a period of 30 min, an incubation period used for testing of effects on platelets. *(FPIA analysis available in supplement B)*

For further experiments, we selected MWCNTs with a 60 nm diameter, M60, as a representative CNT material due to its purity as determined by inductively coupled plasma mass spectrometry (ICP-MS) and transmission electron microscopy (TEM) *(available in supplement D)* and highly reproducible platelet aggregating performance.

The comparison was made among properties of M60 MWCNTs and nC60, which did not influence platelet aggregation at all. The surface charges of both materials in plasma were close to zero, as demonstrated by zeta potential measurements (*supplement D*). The structures of the M60 and nC60 aggregates were determined by electron microscopy (EM); field-emission scanning electron microscopy (FESEM) and TEM showed numerous protuberances on the periphery of the M60 clusters, which were formed by a relatively long, dense net of highly tangled CNTs lacking a specific orientation. In contrast, nC60 particles were largely devoid of these surface features *(supplement D).*

To compare the effect of functionalized carbon nanotubes with their pristine counterparts, we have prepared COOH- functionalized CNTs from M60 nanotubes in house. Carboxylated MWCNTS were prepared by refluxing pristine MWCNTs M60 in a concentrated 3:1 (v/v) H_2SO_4 and HNO_3 mixture at 70°C for 2 hours followed by washing and dialysis in water. Functionalization reduces impurities, provides water solubility and, moreover, allows easier bioconjugation. Characterization was performed by FESEM and the experimental protocols were same as for pristine CNTs *(supplement G).*

3.2. Blood platelets

For all the platelet experiments, platelet rich plasma (PRP) was prepared from blood of healthy donors (ACD anticoagulated, Department of Transfusion Medicine, Clinical Center, NIH, Bethesda, MD). 50 mL of whole blood was centrifuged at 150 *g* for 10 minutes at room temperature and platelet rich plasma (PRP) was collected with Pasteur pipette. The sediment was then centrifuged at 1000 *g* for 15 minutes at room temperature to obtain platelet poor plasma (PPP). The PRP platelet count was assayed (ABX Pentra 60, Horiba ABX, Inc., Irvine, CA) and diluted with PPP to 250 x 10^3 platelets/μL.

The quality of platelets used for experiments is an important issue. Different drugs influence the ability of platelets to aggregate, and methods of blood collection or handling including shear stress or temperature changes have great impact on platelet function in aggregation assays. All experiments performed with unfixed platelet were completed within 4 h after blood collection to ensure normal platelet responsiveness.

3.3. Light transmission aggregometry

To assess the effect of carbon nanotubes on platelet aggregation, we employed light transmission aggregometry (PAP-8E aggregometer, Bio/Data Corp., Horsham, PA). Light transmission aggregometry (LTA) is performed using PRP stirred in an aggregometer cuvette. Transmission of light through the PRP sample is set as 0 % aggregation, while a transmission through platelet-poor plasma (PPP) is set to 100 % (blank). Thus, the aggregation response of platelets after addition of an agonist can be monitored in real time.

PRP and PPP were prepared as mentioned above and used strictly within 4 hours from the collection. All platelet samples were preincubated at 37^{o}C for 2 min in stirring wells of the aggregometer before adding the tested nanomaterials or control solutions, then 20 minutes reading was obtained for every sample set. Thrombin Receptor Activator Peptide (TRAP-6, SFLLRN) (AnaSpec Inc, San Jose, CA), Collagen (Bio/Data Corp., Horsham, PA) and ADP (Bio/Data Corp., Horsham, PA) were used as positive controls. Each experiment was performed using at least 3 blood samples from different donors. Means of maximum aggregation responses ± standard errors of mean (SEM) are presented in results. This way we tested and compared platelet aggregation response to all the available nanomaterials. For further experiments we selected M60 as described in nanomaterial section.

While investigating the mechanism of CNT-induced platelet aggregation, we questioned the role of calcium influx. For all Ca^{2+} influx experiments, whole blood was heparinized with 1 IU/mL heparin (Baxter Healthcare Corp., Deerfield, IL), subsequently $CaCl_2$ (Sigma-Aldrich Inc., St.Louis, MO) was added to the PRP (after adjusting the PLT count) to reach a final Ca^{2+} concentration of 2.5 mM. For experiments concerning inhibitors of platelet calcium signaling pathways, these were prepared as following: SKF 96365 (1-[2-(4-methoxyphenyl)-2-[3-(4methoxyphenyl) propoxy] ethyl] imidazole, Alexis Biochemicals, Axxora Llc., San Diego, CA) was dissolved in Milli-Q water (10 mM). TBHQ (t-butylhydroquinone, Alexis Biochemicals, Axxora Llc., San Diego, CA), MRS2500 (Tocris Bioscience, Ellisville, MO), 2-APB (2-aminoethoxydiphenyl borate, EMD-Calbiochem Brand, San Diego, CA) and DM BAPTA, AM (Invitrogen Corp., Carlsbad,CA) were dissolved in DMSO (Sigma-Aldrich Inc., St.Louis, MO), stock concentrations at 10 mM, NF 449 (Tocris Bioscience, Ellisville, MO) in DMSO at stock concentration 1 mM and stored at -20°C until use. 0.5 M EDTA (Gibco, Grand

Island, NY) was stored at room temperature. Immediately before each experiment, aliquots of inhibitors were thawed, warmed (when applicable) and diluted to a working concentration in H_2O or DMSO. Working concentrations were following: 40 μM DM-BAPTA AM, 1 μM NF 449, 5 nM MRS 2500, 20 μM TBHQ, 10 μM and 100 μM SKF 96365, 100 μM 2-APB. Final concentration of DMSO in PRP was less or equal to 1%, this concentration proved not to influence the platelet aggregation response to CNTs. Upon addition of inhibitors, PRP was agitated gently and incubated at 37°C for 10 minutes prior to testing.

3.4. Analysis of platelet surface activation markers and platelet membrane microparticles (MPs) by flow cytometry

Flow cytometry is a multipurpose tool allowing wide variety of platelet assays (Michelson, 2007). Flow cytometry allows analysis of several thousand elements in one run. Platelets, cells and other particles in the sample flow in a hydrodynamically focused stream of fluid subjected to one or more laser beams of specific wavelengths. The detector in line with the light beam provides for each passing particle a forward scatter (FSC) characteristic, which correlates with the particle volume or size. A detector perpendicular to the light beam records side scatter (SSC) characteristics, which depend on the inner complexity of the cell, like granularity, shape of the nucleus or membrane roughness. Therefore events form characteristic populations on FSC/SSC plot. Additional detectors recognize the fluorescence signal from flowing events, such as platelets labeled with different monoclonal antibodies, each conjugated to a specific fluorophore emitting in a different fluorescence band (Simak, 2009).

To further characterize CNT-induced PLT activation, we investigated PLT surface exposure of activation markers CD62P and CD63 using flow cytometry (Simak et al., 1999). CD62P (P-selectin) is expressed in resting platelets on the membrane of platelet α-granules and it is exposed on the platelet surface after α-granule secretion. It is believed that the activation-dependent increase in platelet surface P-selectin exposure is not reversible over time in vitro (Michelson et al., 2006). However, P-selectin may be released from the platelet surface in a soluble or membrane microparticle (MP) associated form. CD63 is another degranulation dependent platelet surface marker that in resting platelets resides on the membranes of the lysosomes and dense granules (Israels et al., 2007). Thus, the platelet surface exposure of CD63 requires

stronger activation signal compared to CD62P. Membrane microparticles (MPs) are phospholipid vesicles of about 0.1-1 μm in size released from plasma membrane of stimulated platelets and other cell types (Simak and Gelderman, 2006). Platelet MPs expose various platelet membrane antigens and majority of platelet MPs also expose phosphatidylserine, thus being procoagulant and may be prothrombotic in vivo.

In our experiments, PRP was prepared as described above and then diluted to $250x10^3$ platelets/μL with PPP for microparticle experiments and to $30x10^3$ platelets/μL with THB for assessing platelet surface activation markers. (THB, Tyrode's - HEPES buffer, 130 mM NaCl, 2.6 mM KCl, 0.42 mM NaH2PO4, 5.5 mM glucose, 10 mM HEPES, 0.3% bovine serum albumin (BSA), all chemicals were from Sigma-Aldrich Inc., St.Louis, MO) Platelets were equilibrated for 30 minutes after dilution. Then they were stimulated with M60 (100 μg/mL) for 15 min at 37°C with a gentle agitation on the rocking platform. Platelets treated with 20 μM TRAP or PBS (Phosphate buffered saline, Gibco, Grand Island, NY) were used as a positive and negative control, respectively.

For flow cytometric analysis, platelet surface markers were labeled with fluorescent monoclonal antibodies, CD41a (FITC labeled) and CD62P or CD63 respectively (both PE labeled). Matching isotype controls and non-labeled samples were used as controls. Monoclonal antibodies CD41a FITC (clone HIP8), CD62P PE (clone AC1.2), CD63PE (clone H5C6), and corresponding isotype controls (mouse IgG1 kappa, clone X40) were all from BD Bioscience (San Jose, CA). Data were acquired using a FACSCalibur flow cytometer (Becton Dickinson, San Diego, CA) equipped with CELLQuest software with forward scatter and side scatter in logarithmic mode and subsequently analyzed using FlowJo (Tree Star, Inc. Ashland, OR). Expression of platelet activation markers was evaluated as a percentage of CD62P+ and CD63+ platelets.

We investigated whether these antigens were released from platelet surface in membrane microparticles as well. Platelet MPs assays and platelet surface marker analysis were run in parallel, using identical initial blood specimen, both types of samples were stained with the same type of fluorescent monoclonal antibodies. Microparticle samples, after incubation with nanomaterials, were spun for 10 minutes at 10°C at 10000g to obtain platelet free plasma (PFP) for the MP assay. Samples were then processed and analyzed as described previously (Gelderman and Simak, 2008). Aliquots of 50 μL PFP were incubated for 20 min at room

temperature in the dark with saturating concentrations of FITC- and PE-conjugated antibodies. In parallel, nonlabeled samples and samples labeled with relevant isotype controls were analyzed. After incubation and washing with 1 mL HBSS/ Ca^{2+}/BSA (Hank'sbalanced salt solution, Gibco, Grand Island, NY/ 2.5mM $CaCl_2$/ 0.3% BSA), samples were resuspended in 500 µL HBSS/Ca^{2+}/BSA and analyzed by flow cytometry. Data were acquired using the flow cytometer and software as described above. MPs were analyzed using both forward scatter (FSC) and side scatter (SSC) in logarithmic mode. Standard polystyrene nanobeads 200 nm - 1,000 nm from Duke Scientific Corp., Fremont, CA were used for the estimation of MP size. MPs were defined as particles ≤1 μm in size compared on forward scatter with the size standard polystyrene nanobeads of 1 μm in diameter. Counts of CD41a+CD62P+MPs and CD41a+CD63+MPs in the platelet supernatant were evaluated using double fluorescence plots acquired for 60 seconds at the standard flow rate determined by TruCount beads (BD Bioscience San Jose, CA). MPs count per microliter of PRP was calculated.

3.5. Platelet-CNT interaction assessed by Electron microscopy

Platelet morphology and intracellular structure after exposure to the nanomaterials were directly observed by transmission electron microscopy (TEM) and field-emission scanning electron microscopy (FESEM).

Platelet-rich plasma (PRP) was prepared from the blood of healthy donors as described previously and after platelet count adjustment to for 250 x 10^3 platelets/µL, platelets were allowed to equilibrate for 30 min at 37°C. The interaction of nC60 and M60 CNTs with human blood platelets was analyzed by mixing 450 µL platelet stock solution with 50 µL nanoparticle suspension (freshly prepared solution, 1 mg/mL), TRAP or Thapsigargin (TPG, Invitrogen Corp., Carlsbad, CA), (final concentrations were 20 µmol/L and 6 µmol/L, respectively) and incubating at 37°C for 15 min under gentle agitation. The ultrastructural analysis of the CNT-platelet interaction was performed by FESEM and TEM. For FESEM, platelets were fixed with 4% paraformaldehyde (PA) for 30 min, carefully deposited onto clean glass coverslips by cytospin, washed twice with PBS, fixed with 2% glutaraldehyde (GTA), washed extensively with cacodylate buffer, dehydrated in an ethanol series, washed with tetramethylsilane and dried

at room temperature under vacuum. Some samples were sputter-coated with a thin film of gold at 13.3 Pa and 45 mA for 90 s. For the TEM, platelets were fixed in 4% PA and 1% GTA for 1h, postfixed with 4% osmium tetroxide (OsO4) solution in cacodylate buffer, dehydrated in an ethanol series, embedded with Spur and polymerized for 2 days at 65°C. Ultrathin sections (aproximately 60 nm) were cut on a Leica ultramicrotome (Leica Microsystems Inc., Buffalo Grove, IL) and collected onto 600 mesh copper grids. All the electron microsopy specific chemicals were purchased from Electron Microscopy Sciences, Hatfield, PA.

To further explore the possible interaction of CNTs with individual organelles and thus elucidate the mechanism of CNTs effect on platelets, we were able to directly visualize dense tubular system by peroxidase labeling with 3,3'-diaminobenzidine tetrahydrochloride hydrate (DAB)-osmium product (Sigma-Aldrich Inc., St.Louis, MO) (White, 2004). Platelets were fixed with 0.1% GTA in PBS for 15 min, washed twice with PBS to remove the excess plasma proteins, fixed with 2.5% PA and 0.5% GTA for 30 min, washed extensively with 0.05 mol/L Tris buffer and incubated overnight with DAB solution (2.5 mg/mL in 0.05 mol/L Tris buffer) at 4°C. On the following day, the DAB solution was replaced with freshly prepared DAB solution containing 0.003% hydrogen peroxide (Sigma-Aldrich Inc., St.Louis, MO) and incubated for 2 h at RT. The platelets were then extensively washed with cacodylate buffer, postfixed with 4% OsO_4 for 1h at RT in the dark, dehydrated in an ethanol series, embedded in Spur and sectioned using a microtome for TEM.

3.6. Calcium influx in CNT-induced platelet activation

In order to confirm the CNT-induced extracellular Ca^{2+} influx in platelets, we investigated the acute effect of CNTs on intracellular free Ca^{2+} concentration $[Ca^{2+}]i$ in individual platelets loaded with a Ca^{2+} -sensitive probe FURA-2 AM employing ratio fluorometry, method modified for platelets (Simakova and Arispe, 2007).

For Ca^{2+} influx analysis in individual platelets PRP was prepared from heparinized blood and re-calcified as described previously, diluted with PPP to a platelet count $250x10^3$ platelets/μL and incubated with 100 μM acetylsalicylic acid (Sigma-Aldrich Inc., St.Louis, MO) for 30 minutes in 37°C to inhibit platelet activation during the procedure. PRP was than incubated with 2 μM

FURA-2,AM (Invitrogen Corp., Carlsbad, CA) for 1 hour at 37°C. After subsequent washing, platelets were resuspended in 300 μL of THB and incubated for 20 minutes on poly-L-lysine coated coverglass (Sigma-Aldrich Inc., St.Louis, MO). Changes in fluorescence of individual platelets (n = 100) were monitored at 340 nm and 380 nm excitation (the rate of data capture was 170/min) using a Nikon inverted epi-fluorescence/phase microscope equipped with a low-light level integrating CCD camera with a microphotometer assembly (InCyt I/P-2 TM Imaging and Photometry System, Intracellular Imaging Inc., Cincinnati, OH). Real time $[Ca^{2+}]i$ was calculated from the ratio of emission detected at 510 nm at two excitation wavelengths (340 nm and 380 nm) and by comparison to a standard curve established for these settings using buffers of known free Ca^{2+} .

In further experiments, we measured the changes in the Ca^{2+} concentration in the platelet intracellular compartments using Fura FF/AM, a fluorescent probe that is used to measure Ca^{2+} from intracellular stores (Lopez et al., 2006, Wokosin et al, 2004). An increase in the fluorescence of Fura-FF/ AM indicated the depletion of Ca^{2+} from stores.

Qualitative analysis of the Ca^{2+} content in platelets was performed as described previously (Lopez et al., 2006) with some modifications. The PRP was incubated at 37°C with 5 μmol/L Fura-FF/AM and pluronic F-127 (0.025%) (both Invitrogen Corp., Carlsbad, CA) for 45 min, after which 1 μM prostaglandin E1 (Sigma-Aldrich Inc., St.Louis, MO) was added. After 10 min, the cells were collected by centrifugation at 350 g for 10 min and resuspended in a modified intracellular solution containing 20 mmol/L NaCl, 10 mmol/L HEPES-KOH, 120 mmol/L KCl, and 1.13 mmol/L $MgCl_2$, at pH 7.2, supplemented with 40 μg/mL apyrase (all Sigma-Aldrich Inc., St.Louis, MO). Subsequently 100 μmol/L EGTA (Sigma-Aldrich Inc., St.Louis, MO) was added 10 min before the experiment started. Cell membranes were permeabilized, allowing cytosolic Ca^{2+} to be chelated, by mixing 225 μL of Fura-FF/AM-loaded platelets placed in a 96-well plate with 0.5 U/mL streptolysin (Sigma-Aldrich Inc., St.Louis, MO). After 1 min, 25 μL M60, nC60 or Thapsigargin (TPG) (6 μmol/L) solution was added to begin the experiment. Changes in the Ca^{2+} content in platelet stores were monitored by measuring the excitation at 380 nm and emission at 510 nm.

3.7. Underlying molecular mechanism of CNT-induced platelet activation: Store-Operated Calcium Entry (SOCE)

We employed various techniques to support the hypothesis of SOCE involvement in CNTs-induced platelet activation. Experiments on platelet aggregation and calcium influx modification by Ca^{2+} pathway inhibitors were performed as described in previous sections. Further on, we aimed to detect main parts of SOCE system – proteins STIM1 and Orai1 and their localization change after stimulation with CNTs.

SDS-PAGE and Western blot analysis of platelet lysate (Brouckova et al., 2009) confirms the target specificity of the anti-STIM1 and anti-Orai1 antibody used for immunolabeling. Two different anti-STIM1 antibodies were utilized, anti-GOK/STIM1 from BD Bioscience (San Jose, CA), and anti-STIM1 C-terminus from ProSci Inc. (Poway, CA). Binding of the antibodies was visualized using alkaline phosphatase conjugated goat anti-rabbit (GAR) or donkey anti-mouse (DAM) secondary antibodies and BCIP/NBT substrate. (Purchases from Invitrogen Corp., Carlsbad, CA, Jackson ImmunoResearch Laboratories Inc., West Grove, PA, and Thermo Fisher Scientific Inc., Rockford, IL, respectively). Both STIM1 antibodies recognize a band with the molecular weight corresponding to STIM1 (*Supplement D*). Antibody binding was successfully prevented with the blocking peptide for anti-STIM1 and anti-Orai1 antibodies (ProSci Inc.,Poway, CA).

We used TEM and confocal microscopy to visualize STIM and STIM1-Orai1 co-localization in CNTs activated platelets respectively. STIM1 Gold Immunolabeling for TEM was performed as follows: after platelets were incubated with CNTs or TPG, as described above, samples were fixed with 1% PA for 15 min, washed three times with PBS, and permeabilized with 0.1% Triton X-100 (Sigma-Aldrich Inc., St.Louis, MO) for 15 min. After extensive washes with PBS, the platelets were blocked with Image-iT FX signal enhancer (Invitrogen Corp., Carlsbad, CA) for 30 min. The platelets were then incubated with 150 μL of mouse anti-GOK/STIM1 antibody (10 μg/mL) for 2 h, washed 4 times with PBS for 5 min each time, and incubated with 5-nm immunogold-conjugated goat anti-mouse IgG (150 μL, 10 μg/mL) (Invitrogen Corp., Carlsbad, CA) for 2 h at RT. After five washes with PBS for 5 min each, the samples were fixed with 2.0% PA and 2.5% GTA for 30 min at RT to avoid artifacts during the embedding process required for the TEM, as described above. All of the steps were performed at room temperature.

STIM1 and Orai1 in platelets were labeled for laser scanning confocal microscopy (LSCM) using the protocol described above, except the immunogold conjugate was replaced with Alexa Fluor 488-conjugated goat anti-mouse IgG to detect STIM1 and Alexa Fluor 633-conjugated donkey anti-goat IgG to detect Orai1 (both Invitrogen Corp., Carlsbad, CA). After the incubation with the antibodies, the samples were extensively washed with PBS. The platelets were then deposited onto a clean glass slide by cytospin, mounted with VectaShield and imaged with a Zeiss 710 LSM 710 NLO with a Plan Apochromat 100x/1.40 oil objective (Carl Zeiss MicroImaging GmbH, Germany). Once adjusted, the laser configuration and pinhole aperture were kept the same for all samples analyzed. MatLab and Image J software were used for image deconvolution.

3.8. PAMAM dendrimers model

Four generations (G3, G4, G5 and G6) of polyamidoamine (PAMAM) dendrimers from NIST (National Institute of Standards and Technology, Gaithersburg, MD) with etylenediamine core, functionalized with succinamic acid, amine and ethanolamine groups were used in this study (fig.3). The aim was to evaluate the effect of nanoparticle charge and size on platelet-nanoparticle interaction. In dendrimers, both variable characteristics are easily modified. Our laboratory was testing G3 and G6 cationic PAMAM dendrimers.

We performed analysis of dendrimer-induced platelet aggregation by light transmission aggregometry. Platelets were prepared as described previously and the experiments were performed as other aggregometry studies. First we tested all G3 to G6 amine-terminated PAMAM dendrimers with cationic surface at concentration 100 μg/mL. Further on we focused on comparison of “small” G3 and “large” G6. G6 amine-terminated PAMAM dendrimers, were then tested at four concentrations 12.5-100 μg/mL, TRAP and PBS were used as positive and negative controls, respectively.

We also analyzed the expression of platelet activation markers and platelet membrane microparticles by flow cytometry. Flow cytometric analysis of platelets treated with G3 and G6 amine-terminated dendrimers was performed by assessing the expression of CD62P. Platelets were incubated with dendrimers at concentration 25 μg/mL for 20 min at 37^{o}C. 20μM TRAP

treated platelets and PRP only were used as positive and negative control, respectively. Three independent experiments with platelets from different donors were performed. For platelet microparticle experiments, the same incubation conditions and the same controls were used. Both types flow cytometry experiments were otherwise performed as described in Flow Cytometry section.

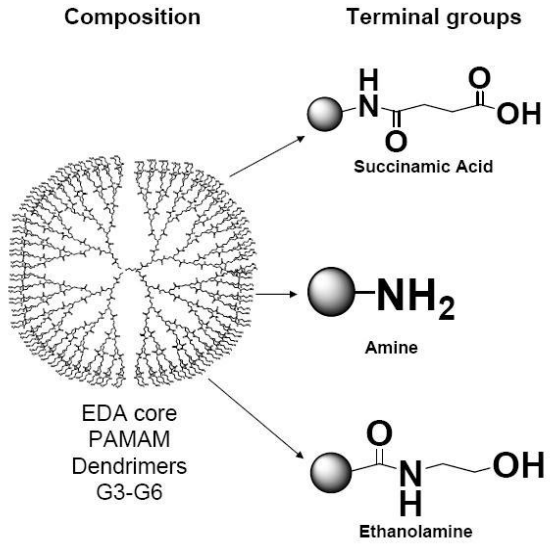

Fig.3. Schematic representation of PAMAM dendrimers. Four generations (G3, G4, G5 and G6) of PAMAM dendrimers with etylenediamine core, functionalized with succinamic acid, amine and ethanolamine groups were used in published study. PAMAM – polyamidoamine.

4. Results

Light transmission aggregometry demonstrated that all tested CNTs produced significant platelet aggregation activity in PRP (Figure 4). At the tested concentration 100 μg/mL, the single-walled carbon nanotubes (SWCNTs) S15 showed maximum platelet aggregation (34 ± 5%), similar to S30 (32 ±6%) and multiwalled carbon nanotubes (MWCNTs) M60 (27 ± 3%) which was significantly higher compared to ACN (15 ± 2%). In contrast, fullerene nC60, fullerenol C60(OH)24, or polystyrene nanobeads (PBs) did not cause any significant PLT aggregation. Collagen was used as a positive control (100%) for each experiment.

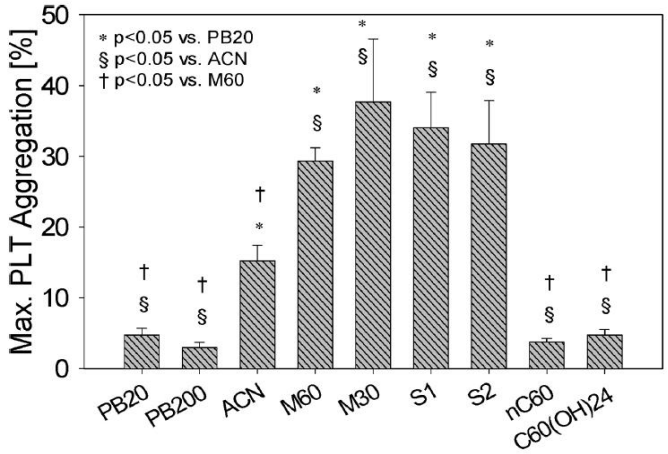

Figure 4. Comparison of platelet aggregating activity of carbon nanomaterials.

Significant difference from standard polystyrene nanobeads (*), amorphous carbon nanopowder ACN (§) and M60 (†) is shown ($p < 0.05$, mean of 5 experiments ± SEM). PB20, PB200 - NIST standard polystyrene nanobeads, ACN - Amorphous carbon nanopowder, M15 – MWCNT with outer diameter 15 +/- 5nm, M60 - MWCNT with outer diameter 60-100nm, MF1(COOH) - MWCNT-functionalized COOH, MF2(NH2) - MWCNT-functionalized NH2, MH – MWCNT with hollow structure, MB MWCNT with bamboo structure, S15 – SWCNT with length 5-15µm, S30 – SWCNT with length 5-30µm, C60 - Fullerene $_n$C60, C60(OH)24 - Fullerenol C60.

For further experiments, we selected MWCNTs with 60-100 nm outer diameter, M60, as a representative CNT material due to its purity and highly reproducible platelet aggregating performance. We have proved that CNTs induce platelet aggregation in a dose-dependent manner. The M60 concentration- dependent PLT aggregation response is shown in Figure 5A.

Since all commercial CNTs contain variable levels of contaminants, particularly heavy metals that can leach into the solution, we tested a potential effect of leachables from M60 material on platelets. When the CNT agglomerates were sedimented at 20 000 g (10 min; 20 °C) from the

suspension of M60 1mg/mL, the supernatant did not induce platelet aggregation (not shown). This result indicates that the CNT agglomerates >0.4 μm observed by FPIA analysis were responsible for M60-induced platelet aggregating activity and that the effect of potential leaching was not significant.

While investigating the mechanism of CNT-induced platelet aggregation, we questioned the role of calcium. Initially we focused on effects of CNTs on intracellular free Ca^{2+} concentration $[Ca^{2+}]i$ in platelets since Ca^{2+} is a key second messenger controlling critical steps in platelet activation. These steps are cytoskeleton reorganization leading to the shape change, degranulation and platelet aggregation. Thus, the increase of $[Ca^{2+}]i$ is essential for platelet activation in the process of hemostasis and thrombosis (Varga-Szabo et al., 2009). Platelets elevate $[Ca^{2+}]i$ by releasing Ca^{2+} from two intracellular stores, dense tubular system and lysosome-like acidic organelles (Jardin et al., 2008). Another way to increase $[Ca^{2+}]i$ is to facilitate Ca^{2+} entry through plasma membrane channels. Performing the experiments in the environment with different Ca^{2+} content showed that the CNT-induced platelet aggregation response is proportional to the extracellular Ca^{2+} concentration (Figure 5B). This finding led us to hypothesize that CNTs induce platelet activation by facilitating extracellular Ca^{2+} influx. In platelets, Ca^{2+} may enter through the plasma membrane by different mechanisms. These include receptor-operated Ca^{2+} entry, second messenger-operated Ca^{2+} entry, and store-operated Ca^{2+} entry (SOCE) (Jardin et al., 2008). The possibility of a nonspecific disintegration of plasma membrane should also be considered.

To characterize the CNT-induced Ca^{2+} influx, we employed inhibitors of platelet calcium signaling pathways. We found that M60-induced platelet aggregation was suppressed with calcium channel blockers SKF 96365 and 2-APB (Figure 5 C,D), results indicating the possible involvement of SOCE. While SKF 96365 has overlapping effects on SOCE and receptor-operated calcium entry, 2-APB has more specific activities, including direct extracellular inhibition of SOCE channels (Ben-Amor et al., 2006, Diver et al., 2001, Bird et al., 2008, Bootman et al., 2002, Marumo et al., 2005, Vostal et al., 1991). In contrast, no effect on M60-induced PLT aggregation response was observed with DM-BAPTA AM (membrane permeant intracellular Ca2+ chelator), NF 449 (P2X1 receptor blocker), MRS 2500 (P2Y1 receptor blocker), or TBHQ (SERCA3 blocker) (data not shown).

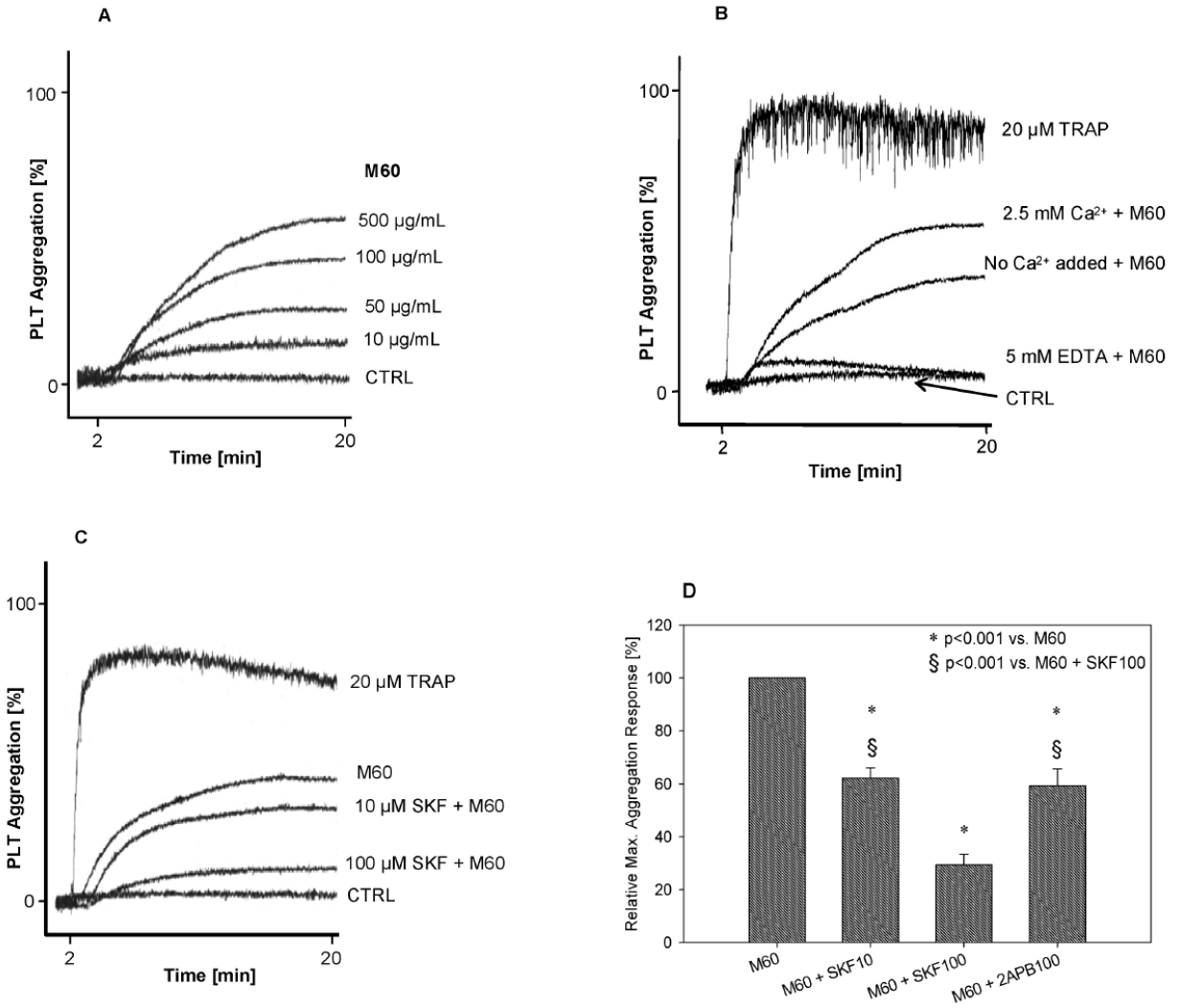

Figure 5. Platelet aggregation induced by multiwalled carbon nanotubes M60. (A) M60 concentration-dependent PLT aggregation response. (B) PLT aggregation response induced by M60 (100 μg/mL) was proportional to the extracellular Ca^{2+} concentration. (C) Calcium entry blocker SKF 96365 inhibited PLT aggregation induced by M60 (100 μg/mL) in a dose dependent manner. PRP with 1 IU/mL heparin and 2.5 mM Ca2+ was used if not otherwise indicated. Representative traces of the light transmission aggregometry experiments (n = 3) are shown. The bar graph (D) shows inhibition of M60-induced platelet aggregation with 10 μM SKF 96365 (M60 + SKF10), 100 μM SKF 96365 (M60 + SKF100), and 100 μM 2-APB (M60 + 2APB100) compared to M60 control without inhibitor (M60). Means + SEM (n =5) of relative maximum aggregation response are shown. CTRL, control platelets treated with vehicle only; CNT, carbon nanotubes; EDTA, ethylenediaminetetraacetic acid; M60, multiwalled carbon nanotubes with outer diameter 60 nm; PLT, platelets; PRP, platelet rich plasma; TRAP, thrombin receptor activating peptide.

To further assess CNT-induced PLT activation, we investigated PLT surface exposure of activation markers CD62P and CD63 using flow cytometry (Simak et al., 1999). CD62P (P-Selectin) is expressed in resting platelets on the membrane of platelet α-granules and it is exposed on the platelet surface after α-granule secretion following platelet activation. CD63 is another degranulation dependent platelet surface marker that in resting platelets resides on the membranes of the lysosomes and dense granules. Platelets were stimulated with M60 (100 μg/mL) or ACN (100 μg/mL), 20 μM TRAP or PBs were used as a positive and negative control, respectively.

M60-induced PLT activation led to significantly higher surface exposure of CD62P and CD63 compared to ACN and untreated platelets. Also, CD62P expression after treatment with ACN differed significantly from untreated platelets (Figure 6). However, the increase in the surface exposure of CD62P and CD63 on M60-stimulated platelets was not as high as expected. Therefore we investigated whether these antigens were released from platelet surface in membrane microparticles. Counts of CD41a+CD62P positive MPs and CD41a+CD63 positive MPs in the platelet supernatant was evaluated using double fluorescence plots are shown in Figure 7A. In contrast to ACN, M60 induced marked release of CD41a+CD62P positive MPs and CD41a+CD63 positive MPs (Figure 7B).

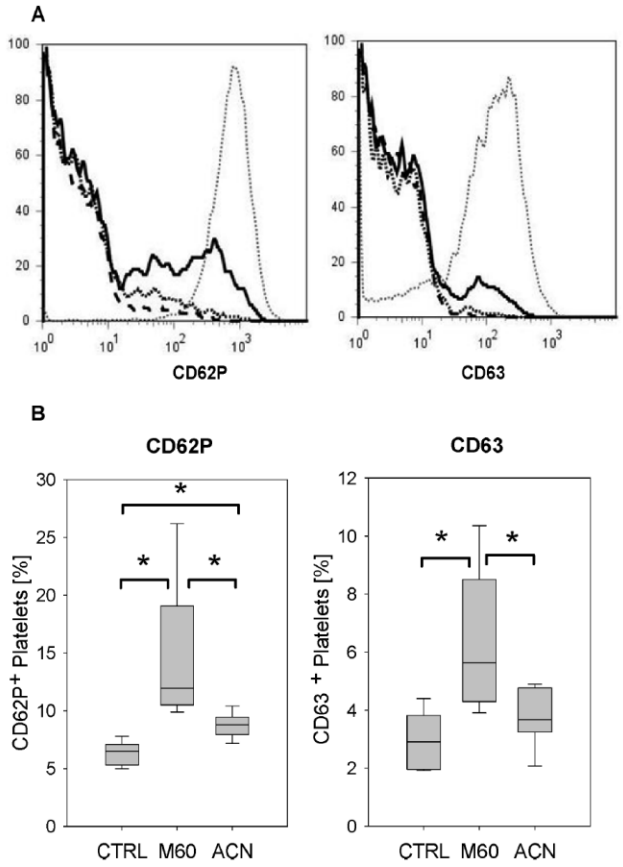

Figure 6. Flow cytometry analysis of platelet surface activation markers. Representative histograms of five experiments are shown (A). M60 (solid line) induced a slight but significant increase in the platelet surface expression of CD62P and CD63 compared to amorphous carbon nanopowder (dotted line) and untreated platelets (dashed line). 20uM TRAP was used as a positive control (gray dotted line). Percentage of CD62P+ and CD63+ platelets is shown on box and whiskers plots (B) indicating the median (full line), the 25-75th and the 10-90th percentiles of the group distribution as boxes and error bars, respectively (n = 5); * p<0.05. M60, multiwalled carbon nanotubes with outer diameter 60 nm; ACN, amorphous carbon nanopowder; CTRL, control platelets treated with vehicle only; TRAP, thrombin receptor activating peptide.

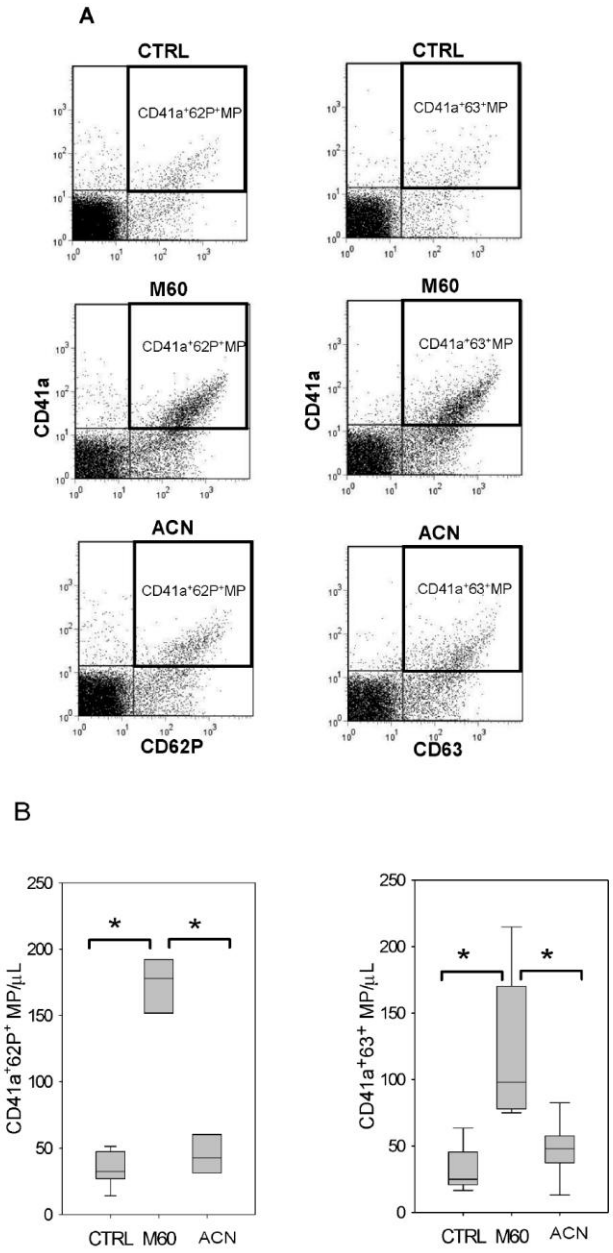

Figure 7. Flow cytometry analysis of platelet membrane microparticles. M60 induced significant release of CD41a+CD62P+ and CD41a+CD63+ platelet membrane microparticles compared to ACN and CTRL. Representative double fluorescence dot plots (A) of five experiments show gated MP positive for CD41a+CD62P+ and CD41a+CD63+, respectively. Counts of released CD41a+CD62P+MP and CD41a+CD63+MP are shown on box and whiskers plots (B) indicating the median (full line), the 25-75th and the 10-90th percentiles of the group distribution as boxes and error bars, respectively (n = 5); *p<0.05. MP, microparticles

For direct visualization of platelet-CNP interaction we used electron microscopy. Platelet morphology and intracellular structure after exposure to these nanomaterials were directly observed by TEM and FESEM. Figures 8a through 8e show the detailed topography of blood platelets exposed to different insults. The morphologies of nontreated platelets and platelets treated with nC60 are typical of the nonactivated state, that is, the platelets have a smooth surface and discoid shape (Jackson, 2007). The maximum platelet activation (positive control), as evidenced by strong aggregation, was achieved by treating platelets with thrombin receptor-activating peptide (TRAP) (Simak et al., 1999, Furman et al., 1998). M60 clearly induced similar platelet morphological changes, pseudopodia formation, membrane budding, and the release of membrane microparticles (MP), as shown in Figure 8e and Figure 8g. TEM and FESEM show that M60 CNTs interact with the platelet plasma membrane (PM) and are translocated into the cytosol, as observed in other cell lines (Figure 8f) (Becker et al., 2007, Porter et al., 2007). Although nC60 is also internalized (Figure 8h), it does not cause significant platelet activation.

Carboxylated carbon nanotubes M60-COOH, although well dispersed in PBS, formed agglomerates in plasma and clearly, as documented by FESEM, induced platelet activation to the same degree as their pristine counterparts *(supplement G)*.

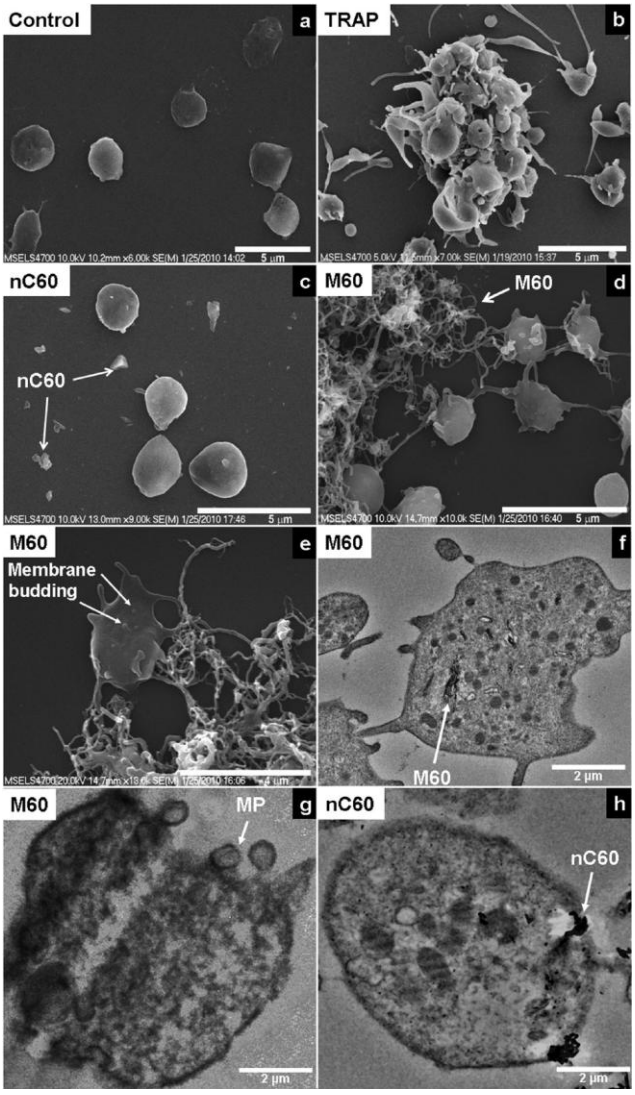

Figure 8. Electron microscopy study of CNTs – PLT interaction. FESEM reveals morphological details of resting platelets (a) or platelets activated with TRAP (positive control) (b) or treated with 100 µg/mL of nC60 (c) or M60 (d). M60 induces membrane budding (e). TEM images of platelet cross sections showing the internalization of M60 (f) with pseudopodia formation, release of MP (g), and internalization of nC60 (h), which does not induce platelet activation.

As shown in flow cytometry and electron microscopy experiments, CNTs activate platelets and cause exposure of surface activation markers, shape change, membrane budding and microparticle release. An essential event during platelet activation is an increase in intracellular free calcium Ca^{2+}. In aggregation experiments, we have already questioned involvement of Ca^{2+} influx on the CNT-induced platelet activation by employing various calcium pathways inhibitors, suggesting the role of SOCE (Store-operated calcium entry).

In order to confirm the CNT-induced extracellular Ca^{2+} influx in platelets, we investigated the acute effect of CNTs on intracellular free Ca^{2+} concentration $[Ca^{2+}]i$ in individual platelets loaded with a Ca^{2+}-sensitive probe FURA2,AM employing ratio fluorometry (Simakova and Arispe, 2007). We demonstrated that M60 induced a rapid concentration-dependent increase in platelet $[Ca^{2+}]i$ indicative of Ca^{2+} entry (Figure 9). The increase of $[Ca^{2+}]i$ above base level was 90±4 nM immediately upon addition of M60. In contrast, after administration of 100 μg/mL ACN or PBs no changes in $[Ca^{2+}]i$ were detected. Also, there was no response to M60 observed in experiments conducted in a calcium free condition, confirming the extracellular origin of Ca^{2+} (data not shown). Moreover, in agreement with the platelet aggregation experiment results, no Ca^{2+} influx was observed when platelets were pretreated with 10 μM calcium entry blocker SKF 96365 (Figure 9).

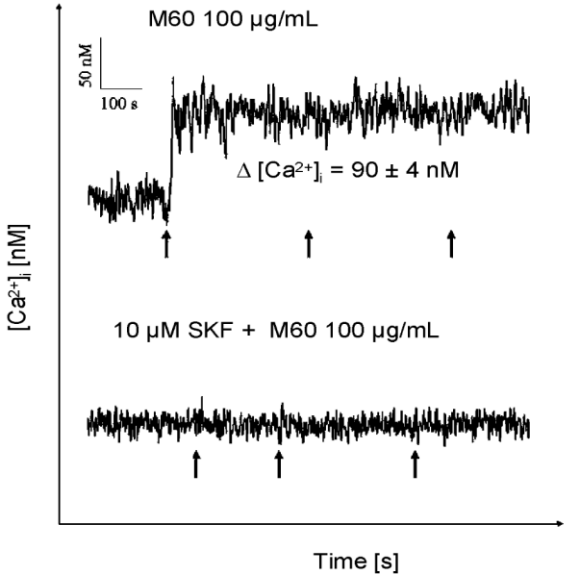

Figure 9. M60-induced rapid elevation of intracellular calcium in platelets as measured by ratio fluorometry of PLT loaded with FURA-2AM. Ca^{2+} influx could be completely inhibited with 10 μM SKF 96365 (10 min preincubation). There was no increase in $[Ca^{2+}]i$ observed in PLT treated with ACN or PBs, neither with M60 in Ca^{2+} free conditions (data not shown). Response of 100 PLT was evaluated in each experiment (n = 3). Representative tracing of responding PLTs from one experiment is shown. Arrows indicate the addition of M60 (100 μg/mL final concentration per dose).

In previous experiments, we have shown that CNT-induced platelet activation follows the influx of extracellular Ca^{2+}. TEM and FESEM showed that M60 CNTs interact with the platelet plasma membrane (PM). Injury of the membrane could cause passive Ca^{2+} efflux from the extracellular environment. However, the fact that we were able to block the CNT-induced calcium efflux with the blockers targeting SOCE mechanism does not support this purely mechanistic theory.

Store-operated calcium entry (SOCE) is the leading mechanism for Ca^{2+} entry in platelets, it is a process controlled by the Ca^{2+} concentrations in the intracellular Ca^{2+} stores (Redondo et al., 2008). The DTS (Dense Tubular System, similar to the endoplasmic reticulum in other cells) is the major source of Ca^{2+} in platelets (Jardin et al., 2008) and the depletion of Ca^{2+} from the DTS triggers the activation of SOCE channel in the plasma membrane to allow the influx of extracellular Ca^{2+}(Varga-Szabo et al., 2009).

Having entered the platelets, M60 could induce mechanical injury (rupture) of DTS membranes or stimulate a local phase transition in the membrane phospholipid structure (Wallace et al., 2008). Both processes could lead to the depletion of Ca^{2+} from the DTS through leakage or passive efflux into the cytosol.

To test this hypothesis, TEM visualizing the DTS was performed by labeling peroxidases present in DTS with 3,3'-diaminobenzidine tetrahydrochloride hydrate (DAB)-osmium product (White, 2004). Figure 10b shows M60 CNTs that are puncturing or in close proximity to the DTS membranes. Next, we measured the changes in the Ca^{2+} concentration in the platelet intracellular compartments using Fura-FF/AM, a fluorescent probe that is used to measure Ca^{2+} from intracellular stores (Lopez et al., 2006, Wokosin et al., 2004). An increase in the fluorescence of Fura-FF/ AM indicated the depletion of Ca^{2+} from intracellular stores, as demonstrated in Figure 10c. M60 and the Sarco-Endoplasmic Reticulum Calcium ATPase (SERCA) pump inhibitor Thapsigargin (TPG) induce a marked decrease in Ca^{2+} in the DTS. SERCA is responsible for refilling the Ca^{2+} stores (Redondo et al., 2008), but in the presence of TPG, SERCA activity is blocked and the luminal Ca^{2+} content is passively effluxed to the cytoplasm. Under the same conditions, nC60 did not induce the depletion of Ca^{2+} from the stores, similar to the untreated platelets.

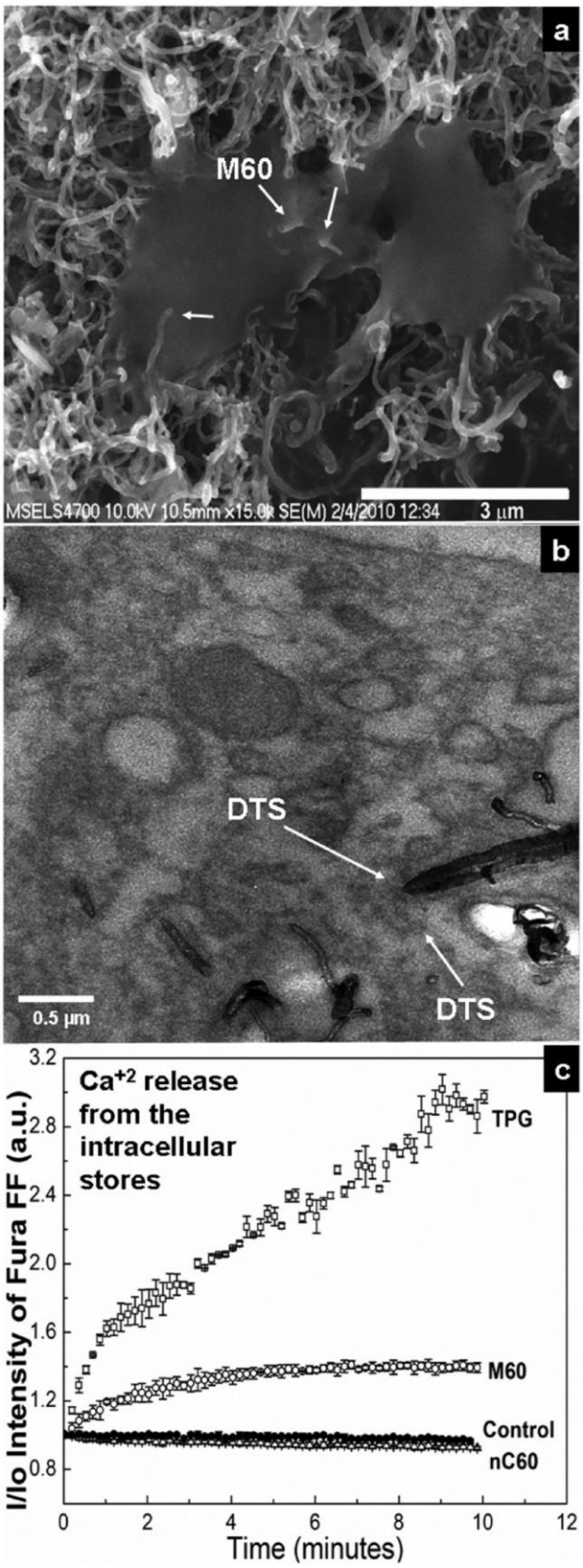

Figure 10. M60 penetrates the platelet plasma membrane and interacts with DTS to cause Ca^{2+} depletion. (a) FESEM image; platelet pseudopodia and CNTs are distinguished by the seeding of platelets without a conductive layer to increase the contrast between M60 and platelets. Peroxidases present in the DTS react with DAB (in the presence of 0.003% hydrogen peroxide), and the osmiophilic product is opaque to the electron beam and provides contrast to the DTS. (b) TEM images of DAB-osmium-labeled platelet DTS. (c) Ca^{2+} release from the intracellular stores of permeabilized platelets (streptolysin 0.5 U/mL and 100 µmol/L EGTA added) measured by Fura-FF/AM. The images are representative of at least three individual experiments with platelets from different donors; error bars represent standard deviations.

The depletion of Ca^{2+} from the DTS is usually not sufficient to activate platelets (Jardin et al., 2008). It is known that SOCE critically regulates platelet activation by allowing the much higher extracellular concentration of Ca^{2+} to enter, which leads to the cytoskeletal reorganization required for the platelet activation (Jardin et al., 2008). Two major factors in SOCE have been identified: the 4-transmembrane-spanning calcium release-activated channel moiety Orai1 and STIM1, a Ca^{2+} sensor expressed predominantly in the DTS (Deng et al., 2009, Wei et al., 2009). STIM1 molecules sense the depletion of Ca^{2+} from the DTS, oligomerize, translocate to junctions adjacent to the plasma membrane, and organize with Orai1 to form the elementary unit of SOCE activation (Deng et al., 2009).

To elucidate whether SOCE has a role in CNT-induced platelet activation, we evaluated the effect of M60 and nC60 on STIM1 aggregation by gold immunolabeling and laser scanning confocal microscopy (LSCM). Western blot analysis confirmed the target specificity of the anti-STIM1 antibody used for immunolabeling *(supplement D)*. Platelets were labeled with 5-nm gold- or Alexa 488-conjugated anti-STIM1 antibody and analyzed by TEM or LSCM respectively.

Figure 11. shows cross sections of platelets labeled with gold anti-STIM1; clusters of STIM1 were present in platelets exposed to TPG or M60, while STIM1 in platelets exposed to nC60 was homogeneously distributed in a manner similar to that of nonactivated control platelets.

LSCM detection (Figure 12.) visualized the clustering of STIM1 and its colocalization with Orai1 at discrete, tightly coupled DTS-PM junctions (Deng et al., 2009) after the treatment of platelets with TPG or M60 CNTs. Thus, our results demonstrate that SOCE plays a key role in CNT- induced platelet activation.

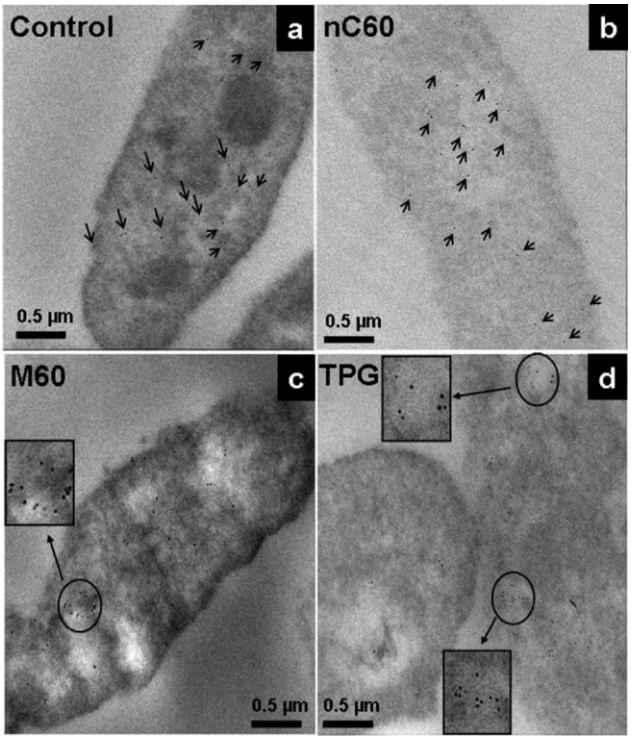

Figure 11. TEM images of 5-nm gold-conjugated anti-STIM1 (anti-GOK/STIM1)-labeled platelets. M60 (100 µg/mL) (c) and TPG (20 µmol/L) (d) induce STIM1 aggregation in platelets, while nC60 (100 µg/mL)-treated platelets (b) show a homogeneous distribution of STIM1 similar to that of the nontreated platelets (a). The images are representative of at least three individual experiments with platelets from different donors.

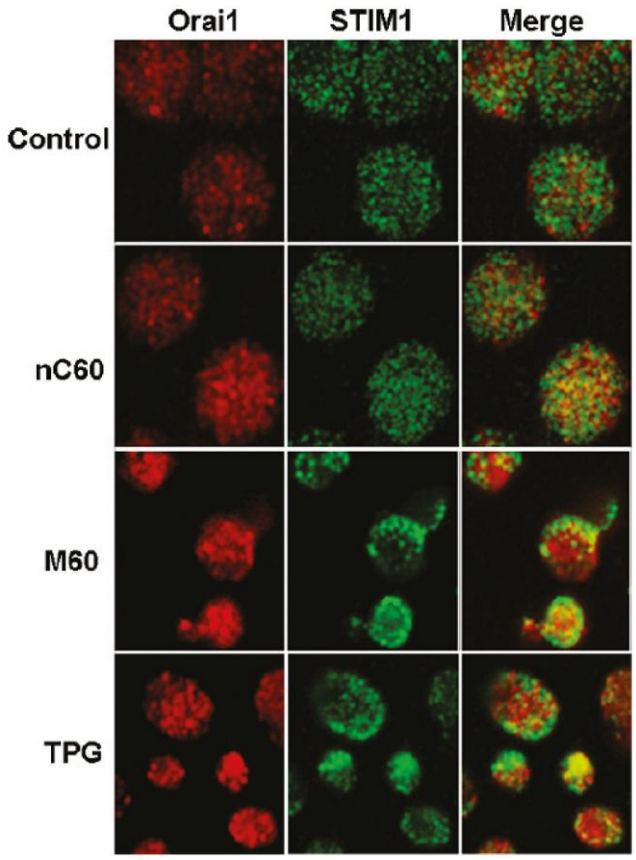

Figure 12. LSCM images of STIM1-(green) and Orai1-(red) labeled platelets. Platelets treated with nC60 show a STIM1 distribution similar to that of the nontreated samples. M60 (100 µg/mL) and TPG (6 µmol/L) induce STIM1 redistribution and colocalization with Orai1 in their discrete, tightly coupled DTS-PM junctions. Yellow in merged images signifies colocalization. The images are representative of at least three individual experiments with platelets from different donors.

To investigate the general effect of size and surface charge of nanomaterial, we used the polyamidoamine (PAMAM) dendrimer model. Dendrimers are spherical large polymer structures, with single compounds symmetrically branching around the core in three-dimensional morphology. Dendrimer chemistry allows synthesis of a wide variety of particles possessing specific properties, suited for the intended use. This quality makes them very good models since characteristics like size (the level of branching – generation) and surface charge (terminal group – type and amount) are easy to manipulate. We tested G3 and G6 generations of amine terminated PAMAM dendrimers with cationic surface, since previous experiments shown no platelet aggregation activity of carboxy- and hydroxyl-terminated counterparts *(supplement E)*. On the other hand, in amine-terminated dendimers platelet aggregation response decreased gradually with decreasing amount of surface amine groups, proving the important role of surface charge (*supplement E)*. To elucidate the role of size, we analysed the dendrimer-induced platelet aggregation by light transmission aggregometry. First, we compared the effect of G3 and G6 generations in concentration 100µg/mL, showing that only G6 induced significant platelet aggregation. G6 was further tested in concentrations ranging from 12.5 to 100µg/mL, proving the dose-response relationship in platelet aggregation response. In addition, we performed flow cytometry analysis of expression of platelet activation marker CD62P after incubation of platelet with G3 and G6 dendrimers in concentration 25µg/mL (fig.13). Interstingly, beside platelet activation, both type of dendrimers caused profound morphological change and membrane derangement, as visualized on characteristic FCS/SSC plot and shift in isotype control binding. The effect was much more pronounced in G6 dendrimers**.** Nor G3 neither G6 induced significant microparticle release compared to the effect of TRAP (fig.14). The reason is probably the dendrimer caused platelet membrane "damage" preceding possible microparticle formation, as this is highly organized process (Simak and Gelderman, 2006, Ahn 2005). We have proved that PAMAM dendrimers are useful in modeling the effects of nanomaterials basic characteristics. Such approach is essential for understanding the specific issues of nanobiocompatibility.

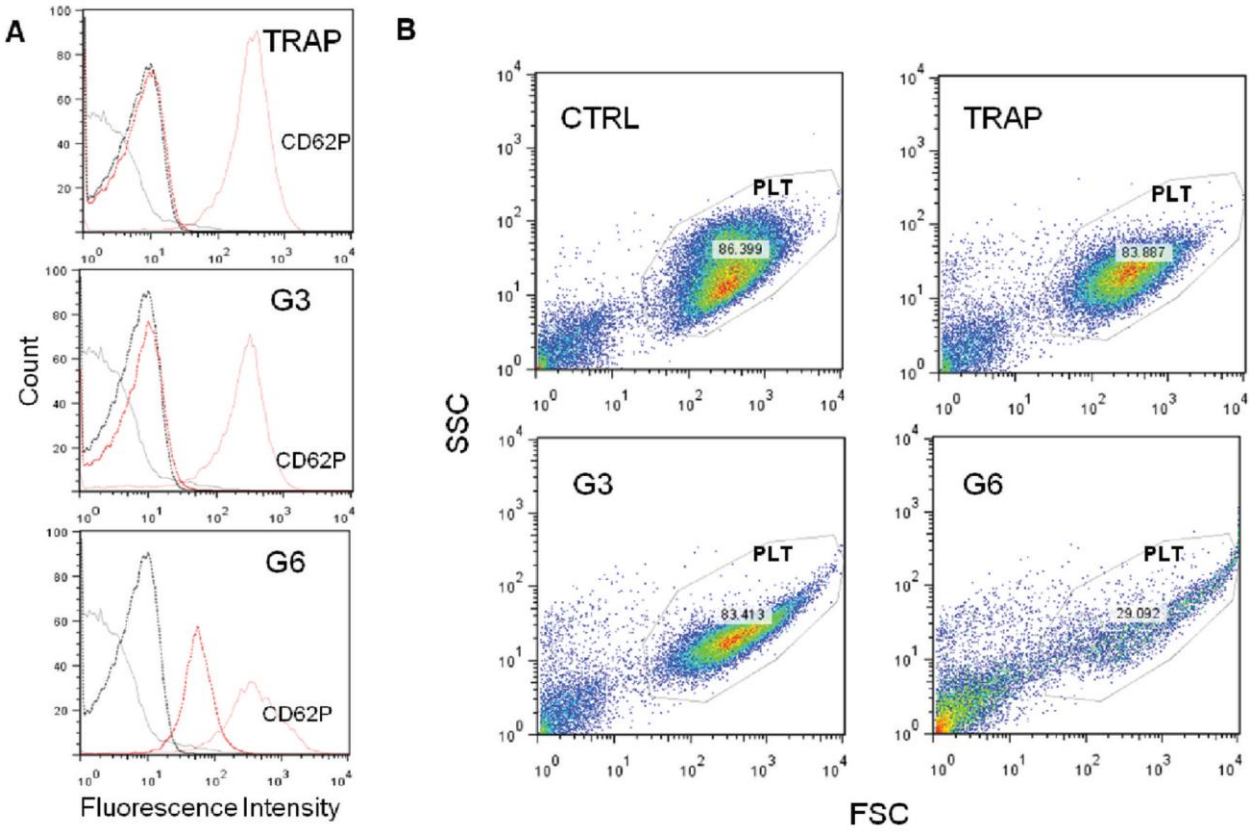

Figure 13. Analysis of expression of platelet activation markers CD62P by flow cytometry in platelets treated with G3 and G6 amine-terminated dendrimers. Platelets were incubated with dendrimers at concentration 25 μg/mL for 20 min at 37 °C. 20 mM TRAP treated plasma and PRP only were used as positive (TRAP) and negative (CTRL) control, respectively. Three independent experiments with platelets from different donors were performed. (A) Expression of PLT activation marker CD62P on dendrimer treated platelets. Representative histograms shown: solid gray line, untreated cells isotype control; dotted black line, untreated cells CD62P; red line, treated cells CD62P; dotted red line, treated cells isotype control; (B) Representative FSC/SSC plots demonstrate significant desintegration of platelets (PLT gate) in G6 treated sample: TRAP, thrombine receptor activating protein (positive control); G3, generation 3 amine-terminated PAMAM dendrimer; G6, generation 6 amine-terminated PAMAM dendrimer; PLT, platelet acquisition gate.

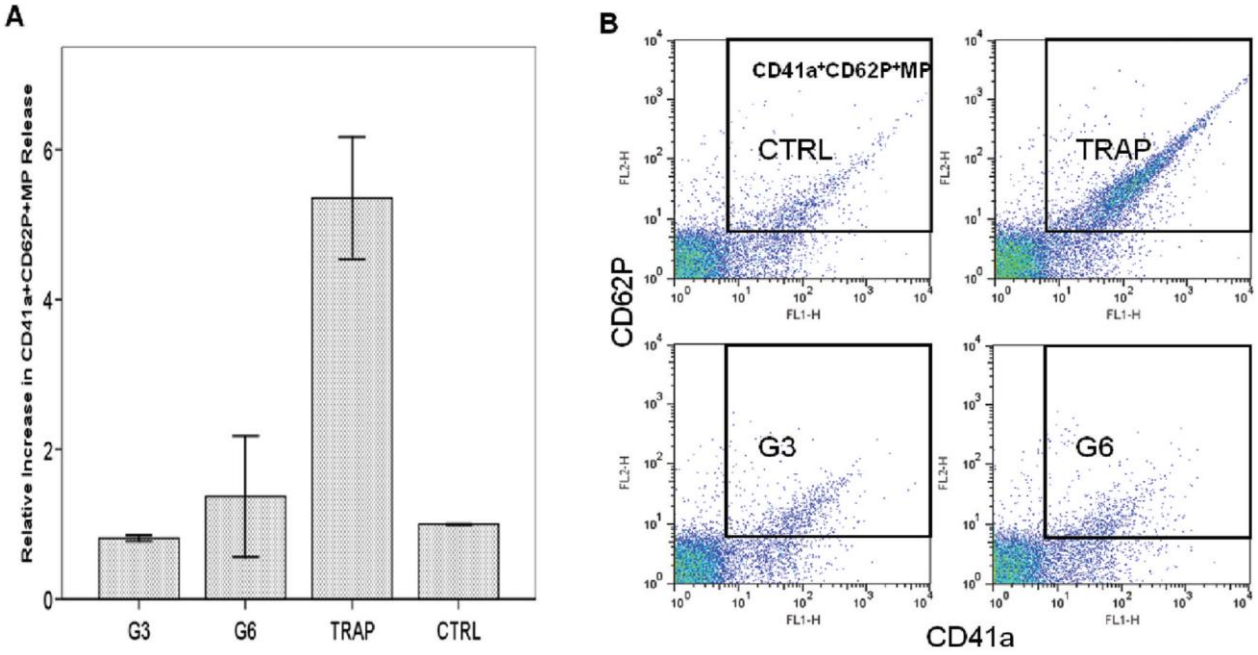

Figure 14. Flow cytometry analysis of the release of platelet membrane microparticles (MP) from dendrimer treated platelets. Platelets were incubated with dendrimers at concentration 25 μg/mL for 20 min at 37 °C; 20 mM TRAP treated plasma and PRP only were used as positive (TRAP) and negative (CTRL) control, respectively. Three independent experiments with platelets from different donors were performed. (A) Relative increase in CD41a + CD62P + MP release; shown is mean ± SEM. (B) Representative double fluorescence plots of platelet CD41a + CD62P + MP: TRAP, thrombine receptor activating protein. (positive control); G3, generation 3 amine-terminated PAMAM dendrimer; G6, generation 6 amine-terminated PAMAM dendrimers.

5. Discussion

As the research to date suggests (Radomski et al., 2006, Bihari et al., 2010, Nemmar et al., 2007, Niwa and Iwai, 2007), CNTs activate platelets and therefore may contribute to the development of thrombotic and other complications. In our experiments we proved that CNTs induce platelet aggregation, activation and marked release of platelet membrane microparticles.

The increase in platelet aggregation activity induced by carbon nanotubes, and not by fullerene, is in agreement with the results published by Radomski *et al* (Radomski et al., 2006). Those investigators reported that mixed carbon nanomaterials (MCN), carbon nanotubes (SWCNT and MWCNT) and standard urban particulate matter (SRM1648) caused activation and aggregation of human platelets, unlike fullerene. The highest aggregation response was induced by MCN, that is a mixture of amorphous carbon with approximately 7% C60. The hypothesis proposed by the investigators (Radomski et al., 2006), that NPs containing amorphous carbon have a higher potential to activate and aggregate platelets compared to crystal-like carbon nanoparticles, is unlikely since our experiments showed that several CNT materials induced a much higher PLT aggregation response compared with amorphous carbon black nanoparticles. This discrepancy emphasizes both the importance of detailed material characterization and, also, the role of different nanoparticle properties like size, shape and surface.

Regarding the shape, one attractive theory is that nanotubes may form interplatelet bridges and as a result promote aggregation, while spherical fullerenes do not. This could be true for single molecules, but is doubtful when considering the agglomerates formation. Bihari *et al*. (Bihari et al., 2010) did also mention the theory of interplatelet connection formed by nanotubes. Those authors discussed the shape of the platelet activation curve, which lacked an initial optical density increase, a characteristic of platelet shape change. Further, the optical density decrease was much slower than when measured following the addition of other platelet activators. The authors (Bihari et al., 2010) raised the question of whether the change in optical density is as a result of a classical platelet agglomeration or whether platelets become connected to each other through SWNT strands. Microscopy experiments performed both by Radomski et al. and our group clearly showed that the platelet morphology changes corresponded with platelet activation. Also, the different aggregation curve shape might be due to the fact that CNTs-induced

aggregation does not run the same pathway as the agonist used (ADP), as supported by the results of experiments with various activation pathways inhibitors.

Radomski *et al*. (Radomski et al., 2006) also showed that all the tested nanoparticles except fullerene induced the activation of GPIIb-IIIa. In addition, MCN, but not other carbon nanomaterials, induced increased surface expression of CD62P and decreased GPIb, both markers of platelet activation. Our results, together with Bihari *et al*. (Bihari et al., 2010) indicate the ability of CNTs to induce platelet activation manifested by significant expression of CD62P (P-selectin) and also CD63. We have also documented the release of platelet membranes microparticles positive for alpha granular and dense granular/lysosomal membrane proteins as evaluated by flow cytometry. In addition, we were able to visualize microparticles formation directly by electron microscopy (FESEM and TEM). So far our study has been the first to show microparticle release after platelet contact with CNTs. Platelet membrane microparticles are of procoagulant nature due to the exposure of phosphatidylserine with the other antigens and therefore may be prothrombotic in vivo (Simak and Gelderman, 2006, Gelderman and Simak, 2008).

Our results demonstrate that CNTs activate human platelets by inducing extracellular Ca^{2+} influx, which is susceptible to SOCE inhibitors 2-APB and SKF 96365. Even though none of the inhibitor abolished the platelet aggregation response completely and their specificity could be questioned (Ben-Amor et al., 2006, Diver et al., 2001, Bird et al., 2008, Bootman et al., 2002., Marumo et al., 2005), the results indicates that the Ca^{2+} influx is not caused by unspecific physical perforation of the platelet membrane but rather by specific interactions of CNTs with membrane structures, cytoskeleton, receptors, and/or channel proteins.

SOCE, also formerly called capacitative calcium entry (CCE), is a biphasic Ca^{2+} signaling process, where release of Ca^{2+} from intracellular storage (dense tubular system in platelets) is followed by the Ca^{2+} entry across the platelet plasma membrane, allowing a much higher extracellular Ca^{2+} concentration to enter (Bird et al., 2008, Putney, 2007, Rosado, 2006). Two major players in SOCE have been identified: the 4-transmembrane spanning calcium release-activated channel moiety Orai1, and STIM1 (Deng et al., 2009), a Ca^{2+} sensor expressed predominantly in the DTS (Wei et al., 2009). STIM1 molecules sense the depletion of Ca^{2+} from

the DTS, oligomerize, translocate to junctions adjacent to the plasma membrane, and organize with Orai1 to form the elementary unit of SOCE activation (Deng et al., 2009).

To elucidate the role of SOCE in CNT-induced platelet activation, we evaluated the effect of CNTs induced STIM1 aggregation by gold immunolabeling and laser scanning confocal microscopy (LSCM). We were able to show STIM1 aggregation and STIM1 redistribution and colocalization with Orai1 in DTS-PM junctions. This finding demonstrates that MWCNTs are able to induce extracellular Ca^{2+} influx in platelets by activation of the store-operated Ca^{2+} entry (SOCE). Therefore it becomes clear that the CNT- induced platelet activation involves alterations in intracellular Ca^{2+} homeostasis rather than pure loss of plasma membrane integrity caused by perforation by CNT.

It would be intuitive to consider that CNTs could injure the PM and cause extracellular Ca^{2+} entry. However, in addition to the experiments with calcium entry inhibitors, our TEM and FESEM data did not reveal plasma membrane (PM) breakage, suggesting that the membrane potentially self-seals around the nanotubes immediately after penetration, as previously reported for other cell types (Wallace et al., 2008, Pogodin et al., 2011, Chen et al., 2007).

On the other hand, we were able to document the interaction of CNTs and Dense Tubular System (DTS) and intracellular Ca^{2+} increase accompanying this phenomenon. The interaction of CNTs with cell membranes is a subject of intense investigation (Yang et al., 2010), but we still lack an in-depth understanding of the mechanism and biological consequences of such interactions. Recent studies have shown that CNTs can induce a membrane local phase transition (Wallace et al., 2008) which is known to cause lipid bilayers to become leaky to Ca^{2+} (Tsvetkova et al., 1999). Interestingly, the cholesterol content in the DTS membrane is 5-fold lower than that in the PM (Fauvel et al., 1986, Menashi et al., 1981). The decreased cholesterol content was shown to decrease membrane resistance to structure "opening" and pore formation (Koronkiewicz et al., 2004), increase the susceptibility of membrane to injury, reduce the resealing rate (Vlahakis et al., 2002), and increase ionic transport (Corvera et al., 1992). Therefore, compared to the PM, the DTS membrane seems to be more vulnerable to local phase transition and injury induced by CNTs. Such an injury, possibly caused by CNTs, may result in the increased passive permeability of Ca^{2+} from DTS which activates SOCE mechanism. As we proved in our

experiments, the M60-induced depletion of Ca^{2+} from DTS stores is slower and less effective comparing to Thapsigargin, but still sufficient to trigger STIM1 clustering and SOCE activation.

Based on these findings, we propose possible molecular mechanism of CNTs induced platelet activation. This consists of nanopenetration of carbon nanotubes without plasma membrane damage, interaction of CNTs with DTS membrane leading to the depletion of Ca^{2+} from DTS stores and thus activation of SOCE mechanism. (fig.15)

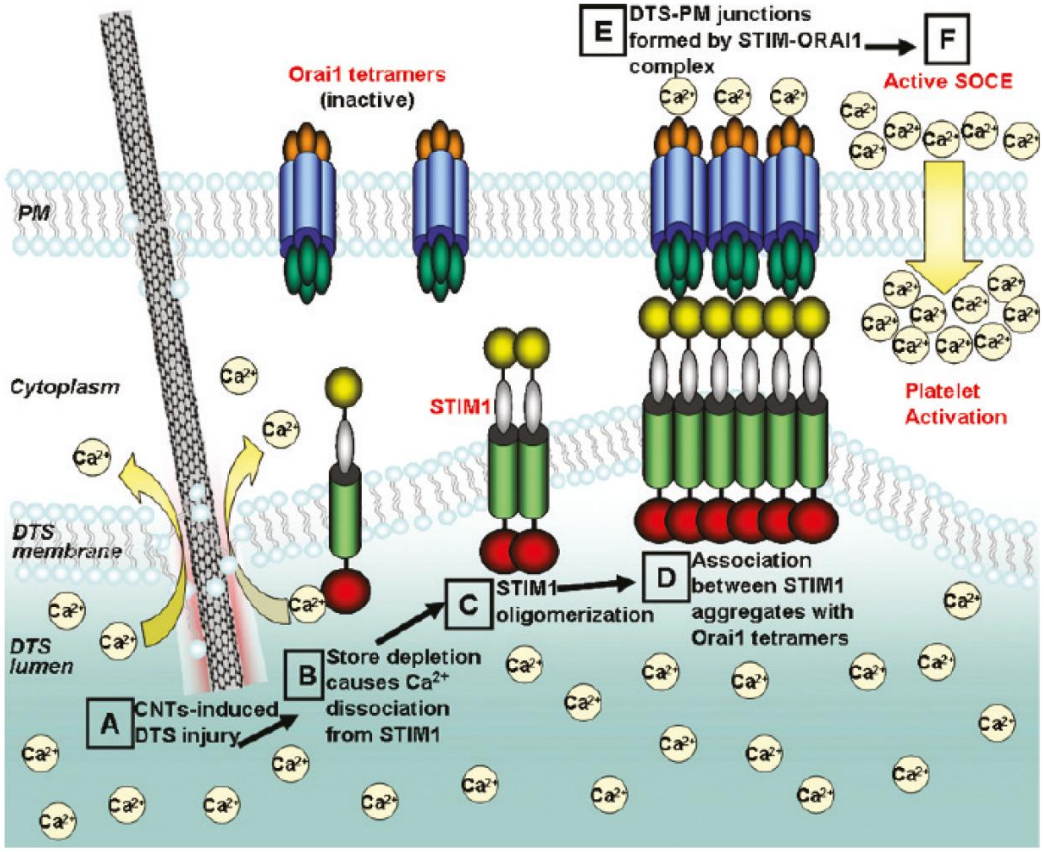

Figure 15. Mechanism of platelet activation by CNTs. (A) CNTs "nanopenetrate" platelets, causing injury to the DTS. (B) Ca^{2+} depletion from the DTS leads to Ca^{2+} dissociation from STIM1, causing (C) STIM1 oligomerization followed by the (D) diffusion, aggregation, and accumulation of STIM1 in DTS - plasma membrane junctions that (E) conformationally gates Orai1 to form a STIM1 - Orai1 complex that (F) activates SOCE for Ca^{2+} influx. (Deng et al., 2009)

Overall our findings could be seen as one "success story", from the observation of the effect through multiple experiments providing crucial information to the elucidation of the underlying mechanism. Thus, the described mechanism of PLT activation might be very unique to the used material – Carbon nanotubes M60. Other investigators described the interference of various nanomaterials with various platelet activation pathways, suggesting different possible activation processes (Radomski et al., 2006, Bihari et al., 2010, Nemmar et al., 2007, Niwa and Iwai, 2007). The Dendrimer study, to which we contributed (*suplemment E)*, revealed that large cationic PAMAM dendrimers induce platelet aggregation through disruption of membrane integrity, thus showing another possible mechanism of nanoparticle-platelet interaction. This study also confirmed that the size and charge play crucial role in nanomaterial effect and that platelet activating mechanism may vary significantly, even within the same class of nanomaterials, proved PAMAM dendrimers as a useful model.

All these findings emphasize that there are no general rules how nanoparticles "behave" in contact with blood. It means that there is a need to test ultra-carefully all the nanomaterials intended for clinical use. The complicating factor is the possible interactions and interference with conventional toxicology assays (Dobrovolskaia et al., 2008, Oberdorster et al., 2005, Dobrovolskaia et al., 2010). Also the reaction with the plasma protein may change nanoparticle reactivity significantly (Lacerda et al., 2010).

The only way to overcome those difficulties to assess nanomaterial safety is the meticulous approach, employing carefully chosen battery of appropriate in vitro and in vivo testing methods. Their results should be confirmed in well designed clinical trials, ideally including also the "second hit" model, since the real patients, severely ill with already dysregulated haemostasis, may profit the most from new diagnostic and therapeutic methods using nanomaterials.

6. Summary and conclusions

In summary, we proved that CNTs induce platelet aggregation, activation and marked release of platelet membrane microparticles. In addition to this, we elucidated the underlying molecular mechanisms for the platelet-activating and potentially thrombogenic effect of pristine MWCNTs. We demonstrated the ability of MWCNTs to nanopenetrate the platelet plasma membrane and interfere with Ca^{2+} homeostasis. MWCNTs caused no discernible plasma membrane damage possibly due to the ability of the lipid bilayer to self-sealing around the nanotubes. However, the interaction of MWCNTs with the DTS caused depletion of Ca^{2+} from the intracellular store. This process was accompanied with STIM1 clustering and its colocalization with Orai1, indicating the activation of SOCE. Thus, SOCE plays a pivotal role in the CNT-induced platelet activation.
Understanding the nature of the interaction of CNTs with platelets will ultimately advance the development of general concepts for designing and testing carbon nanomaterials for optimal biocompatibility in blood.

References:

Ahn YS. Cell-derived microparticles: 'Miniature envoys with many faces'. J Thromb Haemost 3, 884–7, 2005.

Baughman RH, Zakhidov AA, De Heer WA. Carbon nanotubes- the route toward applications. Science 297 (5582), 787–92, 2002.

Becker ML, Fagan JA, Gallant ND, Bauer BJ, Bajpai V, Hobbie EK, Lacerda SH, Migler KB, Jakupciak JP. Length-Dependent Uptake of DNA-Wrapped Single-Walled Carbon Nanotubes. Adv Mater 19, 939–943, 2007.

Ben-Amor N, Redondo PC, Bartegi A, Pariente JA, Salido GM, Rosado JA. A role for 5,6-epoxyeicosatrienoic acid in calcium entry by de novo conformational coupling in human platelets. J Physiol 570 (2), 309–23, 2006.

Bihari P, Holzer M, Praetner M, Fent J, Lerchenberger M, Reichel CA, Rehberg M, Lakatos S, Krombach F. Single-Walled Carbon Nanotubes Activate Platelets and Accelerate Thrombus Formation in the Microcirculation. Toxicology 269, 148–154, 2010.

Bird GS, DeHaven WI, Smyth JT, Putney JW Jr. Methods for studying store-operated calcium entry. Methods 46 (3), 204–12, 2008.

Boero C, Carrara S, Del Vecchio G, Calza L, De Micheli G. Highly Sensitive Carbon Nanotube-Based Sensing for Lactate and Glucose Monitoring in Cell Culture. IEEE Trans Nanobioscience Apr 21 [Epub ahead of print], 2011.

Bootman MD, Collins TJ, Mackenzie L, Roderick HL, Berridge MJ, Peppiatt CM. 2-aminoethoxydiphenyl borate (2- APB) is a reliable blocker of store-operated Ca2+ entry but an inconsistent inhibitor of InsP3-induced Ca2+ release. FASEB J 16 (10), 1145–50, 2002.

Brouckova A, Holada K. Cellular Prion Protein in Blood Platelets Associates with Both Lipid Rafts and the Cytoskeleton. Thromb Haemost 102, 966–974, 2009.

Brukh R, Sae-Khow O, Mitra S. Stabilizing single-walled carbon nanotubes by removal of residual metal catalysts. Chemical Physics Letters 459, (1-6), 149-152, 2008.

Carrara S, Cavallini A, Erokhin V, De Micheli G. Multi-panel drugs detection in human serum for personalized therapy Biosens Bioelectron Mar 17 [Epub ahead of print], 2011.

Chen X, Kis A, Zettl A, Bertozzi C R. A Cell Nanoinjector Based on Carbon Nanotubes. Proc Natl Acad Sci USA 104, 8218–8222, 2007.

Colvin VL. The potential environmental impact of engineered nanomaterials. Nat Biotechnol 21(10), 1166–70, 2003.

Corvera E, Mouritsen OG, Singer MA, Zuckermann MJ. The Permeability and the Effect of Acyl-Chain Length for Phospholipid Bilayers Containing Cholesterol: Theory and Experiment. Biochim Biophys Acta 1107, 261–270, 1992.

Deng X, Wang Y, Zhou Y, Soboloff J, Gill DL. STIM and Orai: Dynamic Intermembrane Coupling to Control Cellular Calcium Signals. J Biol Chem 284, 22501–22505, 2009.

Diver JM, Sage SO, Rosado JA. The inositol trisphosphate receptor antagonist 2-aminoethoxydiphenylborate (2-APB) blocks Ca2+ entry channels in human platelets: cautions for its use in studying Ca2+ influx. Cell Calcium 30 (5), 323–9, 2001.

Dobrovolskaia MA, Aggarwal P, Hall JB, McNeil SE. Preclinical studies to understand nanoparticle interaction with the immune system and its potential effects on nanoparticle biodistribution. Mol Pharm 5(4), 487-95, 2008.

Dobrovolskaia MA, Clogston JD, Neun BW, Hall JB, Patri AK, McNeil SE. Method for analysis of nanoparticle hemolytic properties in vitro. Nano Lett 8(8), 2180–7, 2008.

Dobrovolskaia MA, Neun BW, Clogston JD, Ding H, Ljubimova J, McNeil SE. Ambiguities in applying traditional Limulus amebocyte lysate tests to quantify endotoxin in nanoparticle formulations. Nanomedicine 5(4), 555-62, 2010.

Fauvel J, Chap H, Roques V, Levy-Toledano S, Douste-Blazy L. Biochemical Characterization of Plasma Membranes and Intracellular Membranes Isolated from Human Platelets Using Percoll Gradients. Biochim Biophys Acta 856, 155–164,1986.

Feature. Nature Nanotechnology 1, 8 – 10, 2006.

Fitzgerald KT, Holladay CA, McCarthy C, Power KA, Pandit A, Gallagher WM. Standardization of models and methods used to assess nanoparticles in cardiovascular applications. Small 7(6), 705-17, 2011.

Furman MI, Liu LB, Benoit SE, Becker RC, Barnard MR, Michelson AD. The Cleaved Peptide of the Thrombin Receptor Is a Strong Platelet Agonist. Proc Natl Acad Sci USA 95, 3082–3087, 1998.

Gelderman MP, Simak J. Flow cytometric analysis of cell membrane microparticles. Methods Mol Biol 484, 79-93, 2008.

Gelderman MP, Simakova O, Clogston JD, Patri AK, Siddiqui SF, Vostal AC, Simak J. Adverse effects of fullerenes on endothelial cells: Fullerenol C60(OH)24 induced tissue factor and ICAM-1 membrane expression and apoptosis in vitro. International Journal of Nanomedicine 3(1),2008.

Goldberg M, Langer R, Jia X. Nanostructured materials for applications in drug delivery and tissue engineering. Biomater Sci Polym 18(3), 241–268, 2007.

Hall JB, Dobrovolskaia MA, Patri AK, McNeil SE. Characterization of nanoparticles for therapeutics. Nanomedicine 2(6), 789-803, 2007.

Harrison BS, Atala A. Carbon nanotube applications for tissue engineering. Biomaterials 28(2), 344-53, 2007.

Hou P, Liu C, Cheng H. Purification of carbon nanotubes. Carbon 46, (15), 2003-2025, 2008.

Huang H, Yuan Q, Shah JS, Misra RD. A new family of folate-decorated and carbon nanotube-mediated drug delivery system: Synthesis and drug delivery response. Adv Drug Deliv Rev Apr 13 [Epub ahead of print], 2011.

ISO 10993-4:2002 Biological evaluation of medical devices - Part 4: Selection of tests for interactions with blood.

Israels SJ, McMillan-Ward EM. Platelet tetraspanin complexes and their association with lipid rafts. Thromb Haemost 98 (5), 1081–7, 2007.

Jackson SP. The Growing Complexity of Platelet Aggregation. Blood 109, 5087–5095, 2007.

Jacobs CB, Peairs MJ, Venton BJ. Carbon nanotube based electrochemical sensors for biomolecules. Anal Chim Acta 662(2), 105-27, 2010.

Jardin I, Lopez JJ, Pariente JA, Salido GM, Rosado JA. Intracellular Calcium Release from Human Platelets: Different Messengers for Multiple Stores. Trends Cardiovasc Med 18, 57–61, 2008.

Jardin I, Lopez JJ, Salido GM, Rosado JA. Orai1 mediates the interaction between STIM1 and hTRPC1 and regulates the mode of activation of hTRPC1-forming Ca2+ channels. J Biol Chem 283(37), 25296–304, 2008.

Jin XH, Ishii A, Aoki K, Ishida S, Mukasa K, Ohno S., Detection of human adenovirus hexon antigen using carbon nanotube sensors. J Virol Methods 171(2), 405-7, 2011.

Junt T, Schulze H, Chen Z, Massberg S, Goerge T, Krueger A, Wagner DD, Graf T, Italiano JE Jr., Shivdasani RA, Von Andrian UH. Dynamic visualization of thrombopoiesis within bone marrow. Science 317, 1767–1770, 2007.

Kalbac M, Kavan L, Zukalova M. Nanotuby. Vesmir 87, 846-848, 2008.

Koronkiewicz S, Kalinowski S. Influence of Cholesterol on Electroporation of Bilayer Lipid Membranes: Chronopotentiometric Studies. Biochim Biophys Acta 1661, 196–203, 2004.

Koyama S, Haniu H, Osaka K, Koyama H, Kuroiwa N, Endo M, Kim YA, Hayashi T. Medical application of carbon-nanotube-filled nanocomposites: the microcatheter. Small 2(12), 1406-11, 2006.

Lacerda SH, Park JJ, Meuse C, Pristinski D, Becker ML, Karim A, Douglas JF. Interaction of gold nanoparticles with common human blood proteins. ACS Nano 4(1), 365-79, 2010.

Lam CW, James JT, McCluskey R, Hunter RL. Pulmonary toxicity of single-wall carbon nanotubes in mice 7 and 90 days after intratracheal instillation. Toxicol Sci 77 (1), 126–34, 2004.

Lopez JJ, Redondo PC, Salido GM, Pariente JA, Rosado JA. Two Distinct Ca2+ Compartments Show Differential Sensitivity to Thrombin, ADP and Vasopressin in Human Platelets. Cell Signal 18(3), 373-81, 2006.

Magrez A, Kasas S, Salicio V, Pasquier N, Seo JW, Celio M, Catsicas S, Schwaller B, Forro L. Cellular toxicity of carbonbased nanomaterials. Nano Lett 6(6), 1121–5, 2006.

Manna SK, Sarkar S, Barr J, Wise K, Barrera EV, Jejelowo O, Rice-Ficht AC, Ramesh GT. Single-Walled Carbon Nanotube Induces Oxidative Stress and Activates Nuclear Transcription Factor-KB in Human Keratinocytes. Nano Lett 5(9), 1676-84, 2005.

Marumo M, Wakabayashi I. Monensin augments capacitative Ca2+ entry and subsequent aggregation of platelets via an intracellular alkalosis-mediated mechanism. Pharmacol Res 51 (2), 141– 5, 2005.

Massobrio G, Massobrio P, Martinoia S. Modeling the neuron-carbon nanotube-ISFET junction to investigate the electrophysiological neuronal activity. Nano Lett 8, 4433–4440, 2008.

Medina C, Santos-Martinez MJ, Radomski A, Corrigan OI, Radomski MW. Nanoparticles: pharmacological and toxicological significance. Br J Pharmacol 150 (5), 552–8, 2007.

Menashi S, Weintroub H, Crawford N. Characterization of Human Platelet Surface and Intracellular Membranes Isolated by Free Flow Electrophoresis. J Biol Chem 256, 4095–4101, 1981.

Michelson AD. (ed.) Platelets. Elsevier Inc. New York, 2007.

Michelson AD. Evaluation of platelet function by flow cytometry. Pathophysiol Haemostasis Thromb 35 (1-2), 67–82, 2006.

Moghimi SM, Hunter AC, Murray JC. Nanomedicine: current status and future prospects. FASEB J 19, 311–330, 2005.

Monteiller C, Tran L, MacNee W, Faux S, Jones A, Miller B, Donaldson K. The pro-inflammatory effects of low-toxicity low-solubility particles, nanoparticles and fine particles, on epithelial cells in vitro: the role of surface area. Occup Environ Med 64, 609-15, 2007.

Murthy SK. Nanoparticles in modern medicine: state of the art and future challenges. Int J Nanomedicine 2, 129-47, 2007.

Narayan RJ, Jin C, Menegazzo N, Mizaikoff B, Gerhardt RA, Andara M, Agarwal A, Shih CC, Shih CM, Lin SJ, Su YY. Nanoporous hard carbon membranes for medical applications. J Nanosci Nanotechnol 7(4-5), 1486-93, 2007.

Nemmar A, Hoet P H, Vanquickenborne B, Dinsdale D, Thomeer M, Hoylaerts MF, Vanbilloen H, Mortelmans L, Nemery B. Passage of inhaled particles into the blood circulation in humans. Circulation 105 (4), 411–4, 2002.

Nemmar A, Hoet PH, Vandervoort P, Dinsdale D, Nemery B, Hoylaerts MF. Enhanced peripheral thrombogenicity after lung inflammation is mediated by platelet-leukocyte activation: role of P-selectin. J Thromb Haemost 5, 1217-26, 2007.

Neun BW, Dobrovolskaia MA. Detection and quantitative evaluation of endotoxin contamination in nanoparticle formulations by LAL-based assays. Methods Mol Biol 697, 121-30, 2011.

Neun BW, Dobrovolskaia MA. Method for analysis of nanoparticle hemolytic properties in vitro. Methods Mol Biol 697, 215-24, 2011.

Neun BW, Dobrovolskaia MA. Method for in vitro analysis of nanoparticle thrombogenic properties. Methods Mol Biol 697, 225-35, 2011.

Neun BW, Dobrovolskaia MA. Qualitative analysis of total complement activation by nanoparticles. Methods Mol Biol 697, 237-45, 2011.

Niwa Y, Iwai N. Nanomaterials induce oxidized low-density lipoprotein cellular uptake in macrophages and platelet aggregation. Circ J 71, 437-444, 2007.

Oberdorster G, Maynard A, Donaldson K, Castranova V, Fitzpatrick J, Ausman K, Carter J, Karn B, Kreyling W, Lai D, Olin S, Monteiro-Riviere N, Warheit D, Yang H. Principles for characterizing the potential human health effects from exposure to nanomaterials: elements of a screening strategy. Part Fibre Toxicol 2, 8, 2005.

Pogodin S, Slater NK, Baulin VA. Surface Patterning of Carbon Nanotubes Can Enhance Their Penetration Through a Phospholipid Bilayer. ACS Nano 5, 1141–1146, 2011.

Polizu S, Savadogo O, Poulin P, Yahia L. Applications of carbon nanotubes-based biomaterials in biomedical nanotechnology. J Nanosci Nanotechnol 6(7), 1883-904, 2006.

Porter AE, Gass M, Muller K, Skepper JN, Midgley PA, Welland M. Direct Imaging of Single-Walled Carbon Nanotubes in Cells. Nat Nanotechnol 2, 713–717, 2007.

Putney JW Jr. Recent breakthroughs in the molecular mechanism of capacitative calcium entry (with thoughts on how we got here). Cell Calcium 42(2), 103–10, 2007.

Radomski A, Jurasz P, Alonso-Escolano D, Drews M, Morandi M, Malinski T, Radomski MW. Nanoparticle-induced platelet aggregation and vascular thrombosis. Br J Pharmacol 146 (6), 882–93, 2005.

Redondo PC, Salido GM, Pariente JA, Sage SO, Rosado JA. SERCA 2b and 3 Play a Regulatory Role in Store-Operated Calcium Entry in Human Platelets. Cell Signal 20, 337–346, 2008.

Rosado JA. Discovering the mechanism of capacitative calcium entry. Am J Physiol Cell Physiol 291 (6), C1104-6, 2006.

Rouse JG, Yang J, Ryman-Rasmussen JP, Barron AR, Monteiro-Riviere NA. Effects of mechanical flexion on the penetration of fullerene amino acid-derivatized peptide nanoparticles through skin. Nano Lett 7(1), 155–60, 2007.

Ruggiero A, Villa CH, Holland JP, Sprinkle SR, May C, Lewis JS, Scheinberg D, McDevitt MR. Imaging and treating tumor vasculature with targeted radiolabeled carbon nanotubes. International Journal of Nanomedicine 5, 783–802, 2010.

Ryman-Rasmussen JP, Riviere JE, Monteiro-Riviere NA. Penetration of intact skin by quantum dots with diverse physicochemical properties. Toxicol Sci 91(1), 159–65, 2006.

Shvedova AA, Kisin ER, Porter D, Schulte P, Kagan VE, Fadeel B , Castranova V. Mechanisms of pulmonary toxicity and medical applications of carbon nanotubes: Two faces of Janus. Pharmacology & Therapeutics 121, 192–204O, 2009.

Simak J, Gelderman MP. Cell membrane microparticles in blood and blood products: potentially pathogenic agents and diagnostic markers. Transfusion Med Rev 20 (1), 1–26, 2006.

Simak J, Holada K, Janota J, Stranak Z. Surface expression of major membrane glycoproteins on resting and TRAP-activated neonatal platelets. Pediatr Res 46 (4), 445–9, 1999.

Simak J. Nanotoxicity in blood: effects of engineered nanomaterials on platelets. In Nanotoxicity: from in vivo and in vitro models to health risks. Sahu SC, Casciano DA. (Eds.) John Wiley and Sons Ltd. Chichester, U.K., 191−225, 2009.

Simakova O, Arispe NJ. The cell-selective neurotoxicity of the Alzheimer's Abeta peptide is determined by surface phosphatidylserine and cytosolic ATP levels. Membrane binding is required for Abeta toxicity. J Neurosci 27 (50), 13719–29, 2007.

Smyth SS, McEver RP, Weyrich AS, Morrell CN, Hoffman MR, Arepally GM, French PA, Dauerman HL, Becker RC. Platelet Colloquium Participants, Platelet functions beyond hemostasis. Journal of Thrombosis and Haemostasis 7, 1759–1766, 2009.

Sun TP, Shieh HL, Ching CT, Yao YD, Huang SH, Liu CM, Liu WH, Chen CY. Carbon nanotube composites for glucose biosensor incorporated with reverse iontophoresis function for noninvasive glucose monitoring. Int J Nanomedicine 5, 343-9, 2010.

Tsvetkova NM, Crowe JH, Walker NJ, Crowe LM, Oliver AE, Wolkers WF, Tablin F. Physical Properties of Membrane Fractions Isolated from Human Platelets: Implications for Chilling Induced Platelet Activation. Mol Membr Biol 16, 265–272, 1999.

Varga-Szabo D, Braun A, Nieswandt B. Calcium signaling in platelets. J Thromb Haemost 7 (7), 1057–66, 2009.

Varga-Szabo D, Pleines I, Nieswandt B. Cell Adhesion Mechanisms in Platelets, Arterioscler Thromb Vasc Biol 28, 403-412, 2008.

Veetil JV, Ye K. Tailored Carbon Nanotubes for Tissue Engineering Applications. Biotechnol Prog 25(3), 709–721, 2009.

Vlahakis NE, Schroeder MA, Pagano RE, Hubmayr RD. Role of Deformation-Induced Lipid Trafficking in the Prevention of Plasma Membrane Stress Failure. Am J Respir Crit Care Med 166, 1282–1289, 2002.

Vostal JG, Jackson WL, Shulman NR. Cytosolic and stored calcium antagonistically control tyrosine phosphorylation of specific platelet proteins. J Biol Chem 266 (25), 16911–6, 1991.

Wallace EJ, Sansom MS. Blocking of Carbon Nanotube Based Nanoinjectors by Lipids: A Simulation Study. NanoLett 8, 2751–2756, 2008.

Wei AH, Schoenwaelder SM, Andrews RK, Jackson SP. New Insights into the Haemostatic Function of Platelets. Br J Haemat 147, 415–430, 2009.

White JG. Electron Microscopy Methods for Studying Platelet Structure and Function. Methods Mol Biol 272, 47–63, 2004.

Williams DF. On the mechanisms of biocompatibility. Biomaterials 29(20), 2941-53, 2008.

Williams DF. The Williams dictionary of Biomaterials. Liverpool University Press. 1999.

Wokosin DL, Loughrey CM, Smith GL. Characterization of a Range of Fura-Dyes with Two-Photon Excitation. Biophys J 86, 1726–1738, 2004.

Wu Y, Phillips JA, Liu H, Yang R, Tan W. Carbon nanotubes protect DNA strands during cellular delivery. ACS Nano 2(10), 2023-8, 2008.

Yang K, Ma YQ. Computer Simulation of the Translocation of Nanoparticles with Different Shapes across a Lipid Bilayer. Nat Nanotechnol 5, 579–583, 2010.

www.nano.gov

www.nanoparticles.org

www.nanowerk.com

www.physicstoday.org

List of abbreviations:

2-APB	2-aminoethoxydiphenyl borate
ACB	Amorphous carbon black
ADP	Adenosine diphosphate
BCIP/NBT	5-Bromo-4-chloro-3-indolyl phosphate with nitro blue tetrazolium chloride
C_{60}	Fullerene C_{60}
$C_{60}(OH)_{24}$	Fullerenol
CCE	Capacitative calcium entry
CD15	Cluster of differentiation 15, 3-fucosyl-N-acetyl-lactosamine
CD41	Cluster of differentiation 41, integrin, alpha 2b, platelet glycoprotein IIb
CD41a	Alpha (a) subunit of CD41 (heavy chain; 120 kDa)
CD62P	Cluster of differentiation 62P, P-selectin, Granule Membrane Protein 140
CD63	Cluster of differentiation 63
CNTs	Carbon nanotubes
DAB	3,3'-diaminobenzidine tetrahydrochloride hydrate
DAM	Donkey anti-mouse
DEP	Diesel exhaust particulate
DM BAPTA, AM	5,5-dimethyl BAPTA, AM, selective chelator of intracellular Ca^{2+} stores
DMSO	Dimethyl sulfoxide
DTS	Dense Tubular System
DVT	Deep venous thrombosis
EDTA	Ethylenediaminetetraacetic acid
EGTA	Ethylene glycol tetraacetic acid
EM	Electron microscopy
FESEM	Field emission scanning electron microscopy
FITC	Fluorescein isothiocyanate
FPIA	Flow particle image analysis
FSC	Forward scatter
FURA-2AM	UV light–excitable, ratiometric Ca^{2+} indicator, Fura-2-acetoxymethyl ester
Fura FF/AM	Difluorinated derivative of fura-2
GAR	Goat anti-rabbit

Gõ6976	PKC isoform inhibitor
GPIb	Glycoprotein Ib, platelet surface membrane glycoprotein, CD42
GPIIb-IIIa	Glycoprotein IIb/IIIa , integrin $\alpha_{IIb}\beta_{3,}$ integrin complex on platelets
GPIIIa	Common β subunit (integrin β_3-chain) of the gpIIb/IIIa complex, CD61
GTA	Glutaraldehyde
HUVECs	Human umbilical vein endothelial cells
ICP-MS	Inductively coupled plasma mass spectrometry
ISO	International Organization for Standardization
LSCM	Laser scanning confocal microscopy
LTA	Light transmission aggregometry
MCN	Mixed carbon nanoparticles
MER	Materials and Electrochemical Research Corporation, Tucson, AZ, USA
MI	Myocardial infarction
MMP2	Matrix metalloproteinase 2, gelatinase A
MMP9	Matrix metallopeptidase 9, gelatinase B
MODS	Multiple organ dysfunction
MPs	Membrane microparticles
MRS2500	Selective antagonist of the platelet $P2Y_1$ receptor
MWCNTs	Multiwalled carbon nanotubes
NanoAmor	Nanostructured and Amorphous Materials, Inc., Houston, TX, USA
NanoLab	Nanolab Inc., Waltham, MA, USA
NF 449	Purinergic receptor antagonist that displays high selectivity for $P2X_1$
NF-κB	Nuclear factor kappa-light-chain-enhancer of activated B cells
NIST	National Institute of Standards and Technology
NP	Nanoparticles
PA	Paraformaldehyde
PAC-1	PAC-1 antibody, recognizes epitope on gpIIb/IIIa of activated platelets
PAMAM	Polyamidoamine
PBS	Phosphate buffered saline
PBs	Standard polystyrene nanobeads
PE	Phycoerythrin

PFP	Platelet free plasma
PLT	Platelets
PM	Plasma membrane
PPP	Platelet poor plasma
PRP	Platelet rich plasma
QDs	Quantum dots
ROS	Reactive oxygen species
RT	Room Temperature
SDS-PAGE	Sodium dodecyl sulfate polyacrylamide gel electrophoresis
SERCA	Sarco/endoplasmic reticulum Ca^{2+}-ATPase
SES	SES Research, Houston, TX, USA
SKF 96365	1-[2-(4-methoxyphenyl)-2-[3-(4methoxyphenyl)propoxy]ethyl]imidazole
SOCE	Store-operated Calcium entry
SRM1648	Standard urban particulate matter
SSC	Side scatter
STIM1	Stromal interaction molecule 1
SWCNTs	Single-walled carbon nanotubes
TBHQ	T-butylhydroquinone
TEM	Transmission electron microscopy
THB	Tyrode's buffer
TiO2	Titanium dioxide
TPG	Thapsigargin
TRAP	Thrombin Receptor Activator Peptide

Supplements:

Articles related to the thesis

A. Carbon nanotubes activate blood platelets by inducing extracellular Ca2+ influx sensitive to calcium entry inhibitors. **Semberova J**, De Paoli Lacerda SH, Simakova O, Holada K, Gelderman MP, Simak J. Nano Letters. 2009 Sep; 9(9):3312-7. (IF 2010 12.186)

B. Supporting material for: Carbon nanotubes activate blood platelets by inducing extracellular Ca2+ influx sensitive to calcium entry inhibitors.

C. Carbon Nanotubes Activate Store-Operated Calcium Entry (SOCE) in Human Blood Platelets. De Paoli Lacerda SH, **Semberova J**, Holada K, Simakova O, Hudson SD, Simak J. ACS Nano. 2011 Jul 26;5(7):5808-13. (IF 2010 9.85)

D. Supporting material for: Carbon Nanotubes Activate Store-Operated Calcium Entry (SOCE) in Human Blood Platelets.

E. Nanoparticle Size and Surface Charge Determine Effects of PAMAM Dendrimers on Human Platelets in Vitro. Dobrovolskaia MA, Patri AK, Simak J, Hall JB, **Semberova J**, De Paoli Lacerda SH, McNeil SE. Mol Pharm. 2012 Mar 5;9(3):382-93. Epub 2011 Nov 10. (IF 2010 5.40)

F. Supporting material for: Nanoparticle Size and Surface Charge Determine Effects of PAMAM Dendrimers on Human Platelets in Vitro.

G. Interaction of Carbon nanotubes with human blood platelets. Lacerda SH, **Semberova J**, Holada K, Simakova O, Gelderman MP, Simak J. NSTI-Nanotech Technical Proceedings, Vol 3, 2010: 266-269

Abstracts related to the thesis

H. Carbon Nanotubes Activate Store Operated Calcium Entry (SOCE) In Human Platelets Manifested by STIM1 Capping. Lacerda SH, **Semberova J**, Holada K, Simakova O, and Simak J. Blood (ASH Annual Meeting Abstracts), Nov 2010; 116**:** 3190, Orlando, FLA, USA

I. Ultra-Structural Analysis of the Interaction of Carboxylated Multi-Walled Carbon Nanotubes with Human Blood Platelets. Lacerda SH, **Semberova J**, Holada K, Simakova O, Gelderman-Fuhrmann MP, Simak J. Abstract TH22.505. TechConnect World – Nanotech Conference &Expo, June, 2010, Anaheim, CA,USA

J. Interaction of Nanoparticles with Human Blood Proteins and Platelets. Lacerda SH, **Semberova J**, Simak J. Invited talk. Central Regional meeting of the American Chemical Society, June, 2010, Dayton, Ohio, USA

K. Electron Microscopy Characterization of Platelet Interaction with Carbon nanomaterials. Lacerda SH, **Semberova J**, Simakova O, Holada K, Gelderman MP, Simak J. Journal of Thrombosis and Haemostasis Special Issue: Abstracts of the XXII Congress of the International Society of Thrombosis and Haemostasis, July 2009, Vol 7; S2: 937, Boston, MA, USA

L. Carbon Nanotubes Activate Platelets by Facilitating Extracellular Ca^{2+} Influx. **Semberova J**, Holada K, Simakova O, Gelderman-Fuhrmann MP, and Simak J. Blood (ASH Annual Meeting Abstracts), Nov 2008; 112**:** 992, San Francisco, CA, USA